Invited Speaker

1195 Studying the crystallization of inorganic materials using correlated transmission electron microscopy by Brydson et al
Mr. Rik Drummond-Brydson

Oral Presentation

197 Visualising microstructural dynamics of titanium aluminium nitride coatings under variable-temperature oxidation
Dr Ofentse Makgae[1], Dr Filip Lenrick[2], Dr Volodymyr Bushlya[2], Dr Jon Andersson[3], Dr Rachid M'Saoubi[3], Martin Ek[1]
[1]Centre for Analysis and Synthesis, Lund University, Lund, Sweden, [2]Division of Production and Materials Engineering, Lund University, Lund, Sweden, [3]R&D Materials and Technology Development, Seco Tools AB, Fagersta, Sweden
343 STEM-EELS studies of interfaces between perovskite oxide membranes and single-crystal carrier substrates
Chih-ying Hsu[1,3], Greta Segantini[1], Patrick Blah[2], Graham Kimbell[1], Stefano Gariglio[1], Jean-Marc Triscone[1], Andrea Caviglia[1], Duncan T.L. Alexander[3]
[1]Department of Quantum Matter Physics, University of Geneva, Geneva, Switzerland, [2]Kavli Institute of Nanoscience, Delft University of Technology, Delft, Netherlands , [3]Electron Spectrometry and Microscopy Laboratory (LSME), Institute of Physics (IPHYS), Ecole Polytechnique Fédérale de Lausanne (EPFL), Lausanne, Switzerland
467 High resolution characterization of Y(Mn,In) Blue Chromophoric Oxides
Dr Isobel Bicket[1,2,3], Milenka Andelic[1], Soham Mukherjee[4], Somnath Pal[5], Dipankar Das Sarma[6], Carlo U. Segre[7,8], Gianluigi A. Botton[1,9]
[1]Materials Science and Engineering, McMaster University, Hamilton, Canada, [2]Atominstitut, TU Wien, Vienna, Austria, [3]USTEM, TU Wien, Vienna, Austria, [4]Division of X-ray Photon Science, Department of Physics and Astronomy, Uppsala University, Uppsala, Sweden, [5]MicroNano Systems, Tyndall National Institute, Cork, Ireland, [6]Solid State and Structural Chemistry, Indian Institute of Science, Bangalore, India, [7]Physics & Materials Science and Engineering, Illinois Institute of Technology, Chicago, USA, [8]Center for Synchrotron Radiation Research and Technology, Illinois Institute of Technology, Chicago, USA, [9]Diamond Light Source, Didcot, United Kingdom
669 Phase formation pathways of Me2+ oxides on sapphire (α-Al2O3) substrates
M.Sc. Yasemin Akyol[1], Dr. Sorour Semsari Parapari[2], Prof. Sašo Šturm[2], Prof. Cleva W. Ow-Yang[1,3], Prof. Mehmet Ali Gulgun[1,3]
[1]Materials Science and Nano Engineering, Sabanci University, Tuzla, Istanbul, Turkey, [2]Department for Nanostructured Materials, Jožef Stefan Institute, Jamova Cesta 39, Ljubljana, Slovenia, [3]Sabanci University Nanotechnology Application Center (SUNUM), Tuzla, Istanbul, Turkey
712 Oxygen vacancy imaging in complex oxides by a 4D-STEM optimized virtual detector
Francisco Fernandez Canizares[1,2], PhD. Student Isabel Tenreiro[1], Dr. Hamish Brown[3], Dr. Juan Ignacio Beltran Finez[1], Prof. Alberto Rivera Calzada[1], Prof. Maria Varela[1,2], Dr. Gabriel Sanchez-Santolino[1,2]
[1]Department of Materials Physics, Universidad Complutense de Madrid, Madrid, Spain, [2]Instituto Pluridisciplinar, Universidad Complutense de Madrid, Madrid, Spain, [3]Ian Holmes Imaging Center | Bio21 Molecular Science & Biotechnology Institute, Parkville, Australia
1168 Mapping the Space Charge Region in BaTiO3 and SrTiO3 using 4-Dimensional Scanning Transmission Electron Microscopy
Dr Sangjun Kang[1], Dr Di Wang[2], Dr Dylan Jennings[3], Prof Wolfgang Rheinheimer[4], Prof Christian Kübel[1], Prof Xiaoke Mu[5]

[1]Tu Darmstadt, Darmstadt, Germany, [2]Karlsruhe Institute of Technology , Karlsruhe , Germany, [3]Forschungszentrum Jülich GmbH, Jülich, Germany, [4]University of Stuttgart, Stuttgart, Germany, [5]Lanzhou University, Lanzhou, China

Poster Presentation

20 The behavior of additive manufactured aluminum alloys upon anodization
Lydia Daum[1], Dr. Stefan Ostendorp[1], Dr. Martin Peterlechner[2], Prof. Dr. Gerhard Wilde[1]
[1]Institute of Materials Physics, University of Münster, Münster, Germany, [2]Laboratory of Electron Microscopy, Karlsruhe Institute of Technology, Karlsruhe, Germany
104 Mapping Orthorhombic Domains with Geometrical Phase Analysis
Bernat Mundet[1], Mr. Marios Hadjimichael[2], Jennifer Fowlie[3], Lukas Korosec[4], Lucia Varbaro[4], Claribel Domínguez[4], Prof. Jean-Marc Triscone[4], Duncan Alexander
[1]Catalan Institute of Nanoscience and Nanotechnology (ICN2), Bellaterra, Spain, [2]Department of Physics, University of Warwick, Warwick, United Kingdom, [3]Stanford University, Stanford, USA, [4]Department of Quantum Matter Physics, University of Geneva, Geneva, Switzerland, [5]Electron Spectrometry and Microscopy Laboratory (LSME), Institute of Physics (IPHYS), École Polytechnique Fédérale de Lausanne ole Polytechnique Federal de Lausanne (EPFL), Lausanne, Switzerland
217 In situ observation of dislocation evolution in cerium oxides nanocubes in an environmental TEM
Dr Lucile Joly-Pottuz[1], Dr Rongrong Zhang[1], Dr Thierry Epicier[2], Dr Gaetan Laurens[3], Dr Tristan Albaret[3], Pr Karine Masenelli-Varlot[1]
[1]MATEIS - INSA, , France, [2]IRCELYON - UCBL, , France, [3]ILM - UCBL, , France
362 Transformation of Al2O3 to Cr-rich spinel during spark plasma sintering of alumina dispersed 316L steel
Dr. Zsolt Czigány[1], Dr. Haroune Rachid Ben Zine[1,2], Dr. Csaba Balázsi[1], Dr. Katalin Balázsi[1]
[1]Institute of Technical Physics and Materials Science, HUN-REN Center for Energy Research, Budapest, Hungary, [2]Faculty of Sciences and Technology, Mohamed Khider University, Biskra, Algeria
782 Hybrid electrospun scaffolds for enhanced collagen formation in regeneration processes: electron and confocal microscopy analysis
Dr Joanna Karbowniczek[1], Dr Krzysztof Berniak[1], Prof. Urszula Stachewicz[1]
[1]Faculty of Metals Engineering and Industrial Computer Science, AGH University of Krakow, Krakow, Poland
790 Structural study of perovskite-structure transition metal oxide thin film using Cs-corrected STEM: case of $LaVO_3/DyScO_3$
Chih-ying Hsu[1,2], Clementine Thibault[1], Pau Torruella[2], Jean-Marc Triscone[1], Stefano Gariglio[1], Duncan T.L. Alexander[2]
[1]Department of Quantum Matter Physics, University of Geneva, Geneva, Switzerland, [2]Electron Spectrometry and Microscopy Laboratory (LSME), Institute of Phyiscs (IPHYS), École Polytechnique Fédérale de Lausanne (EPFL), Lausanne, Switzerland
828 Detailed TEM Studies of 1D Nanostructures based on Layered Cobalt Oxide
Dr Raul Arenal[1,2,3], Dr Simon Hettler[1,2], Mrs Kankona Roy[4], Dr. Leela Panchakarla[4]
[1]Instituto de Nanociencia y Materiales de Aragón, CSIC-Universidad de Zaragoza, Zaragoza, Spain., Zaragoza, Spain, [2]Laboratorio de Microscopías Avanzadas, Universidad de Zaragoza. Zaragoza, Spain, Zaragoza, Spain, [3]Araid Foundation, Zaragoza, Spain, Zaragoza, Spain, [4]Department of Chemistry, Indian Institute of Technology Bombay, , Powai, Mumbai, 400076, India
856 The mixed ionic-electronic conductors studied by advanced transmission electron microscopy
Dr Ke Ran[1,2,3], Dr Fanlin Zeng[4], Dr Liudmila Fischer[4], Dr Stefan Baumann[4], Prof Wilhelm Meulenberg[4,5], Dr Kerstin Neuhaus[6], Prof Joachim Mayer[1,2]
[1]RWTH Aachen University, GFE, Aachen, Germany, [2]Forschungszentrum Jülich GmbH, ER-C, Jülich, Germany, [3]Advanced Microelectronic Center Aachen, AMO GmbH, Aachen, Germany,

[4]Forschungszentrum Jülich GmbH, IEK-1, Jülich, Germany, [5]University of Twente, Enschede, The Netherlands, [6]Forschungszentrum Jülich, IEK-12, Jülich, Germany

857 The reversible phase transition of Gd-doped ceria by in situ TEM

Dr Ke Ran[1,2,3], Dr Fanlin Zeng[4], Dr Lei Jin[2], Dr Stefan Baumann[4], Prof Wilhelm Meulenberg[4,5], Prof Joachim Mayer[1,2]
[1]RWTH Aachen University, GFE, Aachen, Germany, [2]Forschungszentrum Jülich GmbH, ER-C, Jülich, Germany, [3]Advanced Microelectronic Center Aachen, AMO GmbH, Aachen, Germany, [4]Forschungszentrum Jülich GmbH, IEK-1, Jülich, Germany, [5]University of Twente, Enschede, The Netherlands

889 Correlation between manufacturing parameters, properties and microstructure in 2D-C/SiC composites

chiara gigante[1], Professor Stefano Poli, PhD Massimiliano Valle, Professor Simone Tumiati, phD Fabio Giacometti, Lorenzo Cavalli, Michela Arnoldi, phD Matteo Boiocchi, phD Yasir Akram, phD Michela Cantù
[1]Earth Science Department A. Desio, Milan, Italy

929 The effects of TiC network microstructure on the mechanical properties of spark plasma sintered Al2O3

Umut Savaci[1], Salih Cagri Ozer[1], Eren Can[1], Yiğit Berkcan Harmankaya[1], Servet Turan[1,2]
[1]Eskisehir Technical University, Department of Materials Science and Engineering, Eskisehir, Turkey, [2]Ceramic Research Center, Eskisehir, Turkey

1006 FIB-SEM/microtoming prepared Cross Section of a Stone Wool Fiber enabling (S)TEM investigation

Phd Student Krestine Hofstedt Rasmussen[1,2], Ph.D Denis V. Okhrimenko[2], Ph.D Louise J. Belmonte[2], Ph.D Dorthe B. Ravnsbæk[3], Ph.D Espen D. Bøjesen[1]
[1]Interdisciplinary Nanoscience Center, Aarhus University, Aarhus, Denmark, [2]ROCKWOOL A/S, Hedehusene, Denmark, [3]Department of Chemistry, Aarhus University, Aarhus, Denmark

1015 The Development of Japanese ceramic ware (pottery and porcelain) Technology as Revealed by EPMA

Dr Rie WAKIMOTO[1], Dr Susumu KAKUBUCHI[2], Dr Sergei Matveev[3]
[1]JEOL Ltd., Musashino Akishima, Japan, [2]SAGA University, SAGA , Japan, [3]JEOL (GERMANY) GmbH, Gute Aenger, Germany

1016 Relative thickness study of TEM samples

Dr Sandra Drev[1], Petra Drnovšek[1], Dr Miran Čeh[1,2]
[1]Center for Electron Microscopy and Microanalysis, Jožef Stefan Institute, Ljubljana, Slovenia, [2]Department for Nanostructured Materials, Jožef Stefan Institute, Ljubljana, Slovenia

1048 The effects of B4C network microstructure on the thermoelectrical properties of spark plasma sintered SiC

Dr Salih Cagri Ozer[1], Ceren Korler[1], Prof. Dr. Servet Turan[1,2]
[1]Eskisehir Technical University, Department of Materials Science and Engineering, Eskisehir, Turkey, [2]Ceramic Research Center, Eskisehir, Turkey

1087 Observing the in-situ formation of the lead-free piezoceramic potassium sodium niobate (KNN) with SAED

Dr Mark Rambaran[1], Dr Daniel Jacobsson[1,2], Dr Sebastian Lehmann[3], Prof. Kimberly Dick[1]
[1]Centre of Analysis and Synthesis and NanoLund, Lund University, Lund, Sweden, [2]National Centre for High Resolution Electron Microscopy , Lund University, Lund, Sweden, [3]Division of Solid State Physics and NanoLund, Lund University, Lund, Sweden

1195

Studying the crystallization of inorganic materials using correlated transmission electron microscopy by Brydson et al

Mr. Rik Drummond-Brydson

PS-09, Lecture Theater 2, august 26, 2024, 14:00 - 16:00

197

Visualising microstructural dynamics of titanium aluminium nitride coatings under variable-temperature oxidation

Dr Ofentse Makgae[1], Dr Filip Lenrick[2], Dr Volodymyr Bushlya[2], Dr Jon Andersson[3], Dr Rachid M'Saoubi[3], Martin Ek[1]
[1]Centre for Analysis and Synthesis, Lund University, Lund, Sweden, [2]Division of Production and Materials Engineering, Lund University, Lund, Sweden, [3]R&D Materials and Technology Development, Seco Tools AB, Fagersta, Sweden

PS-09, Lecture Theater 2, august 26, 2024, 14:00 - 16:00

Background incl. aims
Titanium-aluminium nitride (Ti1-xAlxN) coatings are used to achieve high oxidation and wear resilience in coated metal cutting tools. For the highest performance, the coatings' composition and microstructure are carefully controlled. However, it is difficult to obtain knowledge how these factors effect of the oxidation processes at the microstructural level because studies are most commonly performed: (1) post mortem and cannot observe the structural dynamics underlying the oxide formation in real-time; or (2) averaged over a large volume of the sample (and use powdered materials rather than actual coatings) and lack the spatial resolution to form connections to microstructure. Here, we describe the use of ETEM for visualizing the oxidation process at high spatial and temporal resolution, using technically relevant materials, to provide important insight into where oxidation initiates and how it proceeds to determine the performance of the coating.[1]

Methods
Industrial style Ti1-xAlxN coatings were grown on WC-Co substrates with x = 0, 0.18, 0.44, & 0.67. Samples were prepared through focused ion beam milling (fig. 1a), transferred to MEMS heating chips (Norcada Inc., fig 1b), and finally imaged in ETEM (Hitachi HF3300-S, operated at 300 kV) during heating in an O2 environment (ca. 1 Pa). The samples were observed over a temperature range from 200 to 1000 °C and energy dispersive X-ray spectroscopy (EDX) with pre- and post- elemental mapping by EDX.

Results
The high-frame-rate ETEM movies show that oxidation in TiN proceeds at the grain boundaries and cracks formed during the heating process; in contrast, Ti1-xAlxN coatings transform from large as-deposited grains into oxide nanoparticles. The onset temperature increase with increasing Al content up to x= 0.44, as shown in fig. 1c-s. Moreover, high-resolution ETEM imaging show the presence of anatase TiO2 at the early stages of oxidation across all compositions. Above ~850 °C, the oxide nanoparticles grow through crystal merging, diffusion and recrystallization to form rutile TiO2. The EDX elemental maps coupled with secondary electron imaging reveal a uniform TiO2 sublayer decorated with increasing coverage of Al2O3 particles for x = 0.18 to 0.44. In contrast, coatings with x = 0.67 reveal a complete in-plane phase separation of Al- and Ti-oxides.[1]

Conclusion
The trend with increasing onset temperature for the oxidation with increasing Al content is consistent with the resilience of the corresponding coatings during cutting operations. The in-plane separation observed for the highest Al content (x = 0.67) exposes the softer TiO2 at the surface, and the TiO2-Al2O3 grain boundaries can act as a conduit for oxygen to reach further into the coating; together, these results can rationalise the poorer long-term oxidation resilience resulting from excessive Al.[1] Finally, the study provides insight into the real-time structural dynamics underpinning

the oxidation resistance of Ti1-xAlxN coatings, illustrating how ETEM can uniquely complement other in situ techniques that have recently been applied to these materials.[2,3]

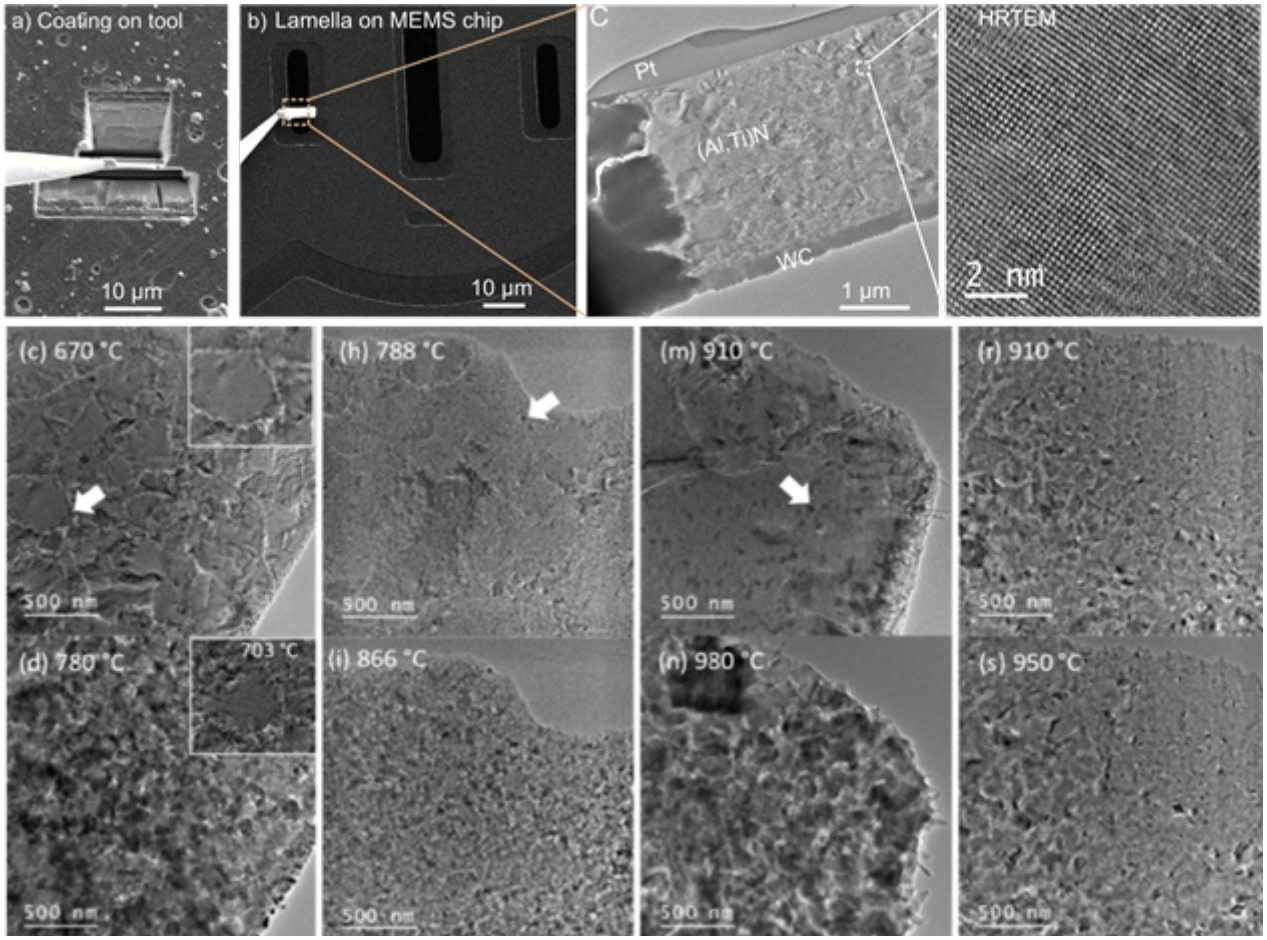

Keywords:

ETEM; TiAlN; coatings; oxidation; tooling

Reference:

[1] O.A. Makgae, F. Lenrick, V. Bushlya, J.M. Andersson, R. M'Saoubi, M. Ek, Appl. Surf. Sci. 618 (2023) 156625. https://doi.org/10.1016/j.apsusc.2023.156625.
[2] C. Saringer et al., Suf. Coatings Technol. 374 (2019) 617
[3] A.B.B. Chaar et al., J. Alloys Compd. 854 (2021) 157205

343

STEM-EELS studies of interfaces between perovskite oxide membranes and single-crystal carrier substrates

Chih-ying Hsu[1,3], Greta Segantini[1], Patrick Blah[2], Graham Kimbell[1], Stefano Gariglio[1], Jean-Marc Triscone[1], Andrea Caviglia[1], Duncan T.L. Alexander[3]
[1]Department of Quantum Matter Physics, University of Geneva, Geneva, Switzerland, [2]Kavli Institute of Nanoscience, Delft University of Technology, Delft, Netherlands , [3]Electron Spectrometry and Microscopy Laboratory (LSME), Institute of Physics (IPHYS), Ecole Polytechnique Fédérale de Lausanne (EPFL), Lausanne, Switzerland

PS-09, Lecture Theater 2, august 26, 2024, 14:00 - 16:00

Perovskite-structure transition metal oxide epitaxial thin films exhibit a variety of functionalities that make them highly promising for the development of novel electronic devices, including non-volatile memories, sensors, and flexible electronics. In recent years, interest has arisen in transforming these thin films into perovskite membranes, that can be detached, transferred and layered similarly to architectures established for 2D materials. Compared to epitaxial heterostructures, this offers potential benefits of, for instance, no structural mismatch strain effects, possibilities to create texture (wrinkles), versatile stacking and, ultimately, scaling down to the 2D limit [1]. Recently, such membrane structures have been studied with Cs-corrected scanning transmission electron microscopy (STEM) using a plan-view geometry [2]. In contrast, here we focus on cross-section studies, where atomic structural quality and flatness/roughness can be precisely assessed. By combining with electron energy-loss spectroscopy (EELS), we further apply this approach with a goal of probing the bonding of membranes transferred to single-crystal substrates, and how this evolves with thermal annealing.
For the measurements, 30 nm-thick $SrTiO_3$ membranes are grown on a 16 nm-thick $Sr_3Al_2O_6$ sacrificial layer on a (001) $SrTiO_3$ substrate using pulsed laser deposition. After dissolving the $Sr_3Al_2O_6$ layer in deionized water, the resulting $SrTiO_3$ membrane is transferred onto a Nb-doped $SrTiO_3$ (001) carrier substrate. This membrane heterostructure is either left “as is”, or is subjected to a thermal annealing at one of a series of temperatures. Focused ion beam milling is then used to prepare a cross-section lamella. These samples are studied in STEM mode using a double-corrected FEI/Thermo Fisher Scientific Titan Themis 60-300, operated at 200 or 300 kV, with STEM-EELS maps recorded in counting mode using a Gatan GIF Continuum ERS equipped with a K3 detector.
By imaging membranes in cross-section from both before and after the steps of $Sr_3Al_2O_6$ dissolution and transfer, it is found that the quality of the $Sr_3Al_2O_6$ sacrificial layer is crucial for final membrane quality, with a flat and uniform $Sr_3Al_2O_6$ layer being necessary for obtaining a flat $SrTiO_3$ film having a high quality of epitaxial growth. The figure shows an example cross-section high angle annular dark-field (HAADF) STEM image of a $SrTiO_3$ membrane transferred to the Nb:$SrTiO_3$ carrier substrate. Because of the twist of the membrane to the carrier substrate, while the cation columns are resolved in the substrate, the membrane depicts only atomic planes. This is, however, still sufficient to study the atomic nature plane-by-plane using Cs-corrected STEM-EELS mapping. Membrane and substrate are separated by a ~2 nm interface gap.
From a STEM-EELS map, the left-hand panels of the figure show EEL spectra of the Ti L-edge and O K-edge, integrated from three different regions: the carrier substrate, the membrane, and also the 2 nm interface gap. It can be seen that there are no significant differences between the membrane and carrier substrate, where the Ti L_3, L_2 peaks show the signature t2g and eg splitting for Ti^4+, and the O K-edges share the same fine structure [3]. To the right of the HAADF image, a line-profile is shown of the Ti L-edge signal extracted across the heterostructure. Surprisingly, the intensity does not decay to zero within the interface gap. Looking at the corresponding EEL spectrum, the lack of splitting in the Ti L_3, L_2 peaks structure indicates that, in the interface gap, Ti exists in a reduced form [4]. This may

be due to the free surface of the membrane and substrate having dangling Ti bonds that are observed in projection.
In summary, we are applying atomic-resolution STEM in a cross-section geometry to study the chemical bonding of transition metal oxide membranes transferred to carrier substrates. By thermally annealing these heterostructures, we expect to create different bonding states between the membrane and the substrate, that will be measured using STEM-EELS.

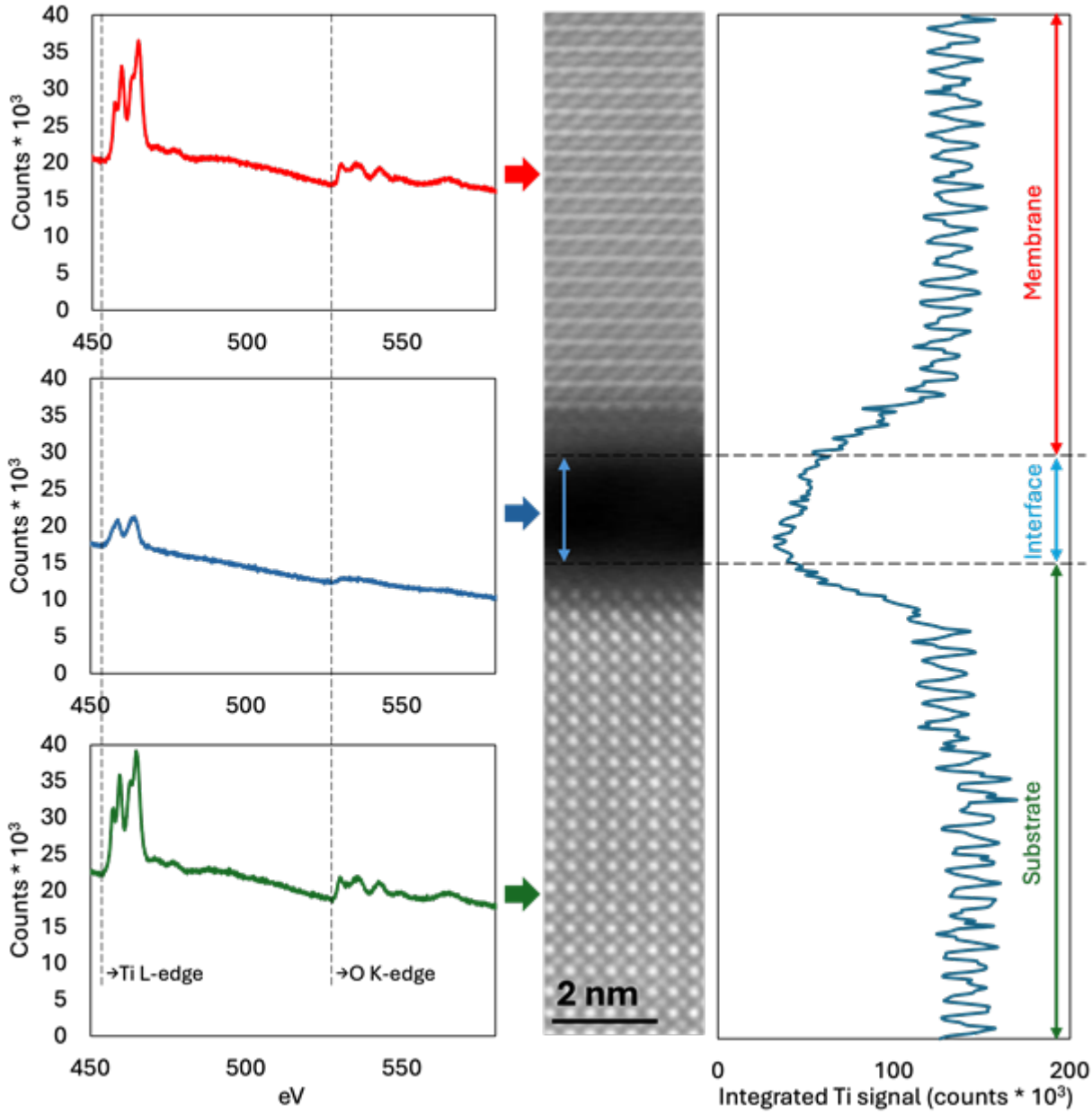

Keywords:

perovskite membrane, EELS, chemical bonding

Reference:

1. A. J. Yang et al., ACS Nano. 17, 9748–9762 (2023).
2. G. Sánchez-Santolino et al., Nature. 626, 529–534 (2024).
3. G. Liu et al., J. Phys. Chem. C. 120, 16681–16686 (2016).
4. E. Stoyanov, F. Langenhorst, G. Steinle-Neumann, American Mineralogist. 92, 577–586 (2007).

467

High resolution characterization of Y(Mn,In) Blue Chromophoric Oxides

Dr Isobel Bicket[1,2,3], Milenka Andelic[1], Soham Mukherjee[4], Somnath Pal[5], Dipankar Das Sarma[6], Carlo U. Segre[7,8], Gianluigi A. Botton[1,9]
[1]Materials Science and Engineering, McMaster University, Hamilton, Canada, [2]Atominstitut, TU Wien, Vienna, Austria, [3]USTEM, TU Wien, Vienna, Austria, [4]Division of X-ray Photon Science, Department of Physics and Astronomy, Uppsala University, Uppsala, Sweden, [5]MicroNano Systems, Tyndall National Institute, Cork, Ireland, [6]Solid State and Structural Chemistry, Indian Institute of Science, Bangalore, India, [7]Physics & Materials Science and Engineering, Illinois Institute of Technology, Chicago, USA, [8]Center for Synchrotron Radiation Research and Technology, Illinois Institute of Technology, Chicago, USA, [9]Diamond Light Source, Didcot, United Kingdom

PS-09, Lecture Theater 2, august 26, 2024, 14:00 - 16:00

Background
Throughout history, bright colours have contributed to the advancement of art and science through inspiring creativity, improving mental wellbeing, and enhancing the transfer of information. However, since many common pigments are produced using toxic materials, there has been a recent burst of interest in producing non-toxic, colourfast, long-lasting pigments for various colour treatment applications [1], led by the discovery of a durable, environmentally friendly inorganic blue pigment Y(Mn_{1-x}In_x)O_3 [2].
The two end compounds of this mixture, $YInO_3$ and $YMnO_3$, are white and black, respectively. Both compounds crystallize in a layered hexagonal lattice, while the intermediate compounds form a solid solution in which In and Mn occupy the same lattice sites. Mixing a small amount of Mn into the $YInO_3$ lattice results in a startling blue colour originating from absorption of other colours by electronic transitions from the Mn 3d states, including nominally forbidden d-d transitions. These transitions are made possible by the non-centrosymmetric trigonal biypramidal (TBP) environment of O around the Mn ions [2,3].
In this study, we present a thorough characterization of the structural and spectral characteristics of Y(Mn_{1-x}In_x)O_3 across the full compositional range. We discuss the origin of the strong blue colour and its correlation with the crystallographic properties of this oxide material.

Methods
We use a Nion HERMES100 STEM operated at 60 keV, with an average energy resolution of 5 meV, to acquire high resolution EEL spectra across a broad range of the electromagnetic spectrum: from the mid-IR to the UV and core-loss regions. We complement our EELS results with high resolution imaging of the crystal structure using STEM, EDS, and iDPC on a double-corrected ThermoFisher Spectra Ultra STEM operated at 200 keV. JEMS enables us to visualize the crystal structure and simulate HAADF images of the various orientations we find in the STEM.

Results
In our EEL spectra, we observe several trends in the mid-IR to UV regions of the spectrum. In the mid-IR, the phonon modes redshift with more In content due to the larger relative atomic mass and size of In compared to Mn. In the visible region of the spectrum, $YMnO_3$ has strong extinction peaks arising from Mn 3d transitions (Fig. 1A), resulting in broadband absorption across the visible spectrum and a black colour in the bulk material. $YInO_3$, on the other hand, has no peaks in this spectral regime until the bandgap onset in the near-UV, resulting in a material which reflects all colours of light and appears white. In the intermediate compounds, such as Y(Mn_{0.1}In_{0.9})O_3, we observe a small peak around 2.2 eV and a change in the higher energy bandgap onset relative to the pure In compound. Further increasing the Mn

fraction results in stronger intensity on the 2.2 eV peak, and a new peak at 1.9 eV which redshifts to 1.7 eV and dominates the lower energy part of this spectrum. Additional extinction signal also arises near the bandgap onset, which overall shifts to lower energy and results in absorption of purple and UV light. This combination of transitions leaves only blue light to be reflected.

Through HR-STEM-EDS, we are able to identify the lattice sites occupied by Mn even in samples with low In concentration, such as Y(Mn_{0.9}In_{0.1})O_3 (Fig. 1B). From our EDS results, we observe that the Mn and In occupy the same lattice sites, substituting for each other in a disordered fashion, for the most part. One notable exception that we have observed is in the Y(Mn_{0.5}In_{0.5})O_3 oxide, wherein the Mn ions are distinctly noted to occupy specific lattice sites in a unit cell larger than former studies suggest (Fig. 1C), whereas the In ions do not show the same behaviour in this lattice. The origins of this mysterious ordering remain to be understood.

Through further analysis of our HR-STEM images, we observe an anisotropic expansion of the crystal lattice as Mn ions are replaced with the larger In ions. The lattice exhibits more expansion along the apical than the basal directions, with the c lattice parameter increasing by 1 Å in $YInO_3$ compared to $YMnO_3$. We observe through selected area diffraction that in several of the intermediate compounds, the crystal lattice has a twist, likely due to the mismatch in size of the substitutional Mn and In ions. Further, using iDPC imaging, we are able to observe distinct structural features in alternating lattice planes, with a repetition matching the size of the system's unit cell (Fig. 1D).

Conclusion

In conclusion, we present a thorough characterization of the blue chromophoric oxide, hexagonal Y(Mn_{1-x}In_x)O_3. We examine the crystallographic and spectral characteristics of the material across the range of compositions to understand the origin of the optical properties that make this such an attractive pigment. We directly confirm the trends observed in x-ray based studies of this material and uncover evidence of Mn ions preferentially occupying unexpected sites in a larger supercell in Y(Mn_{0.5}In_{0.5})O_3.

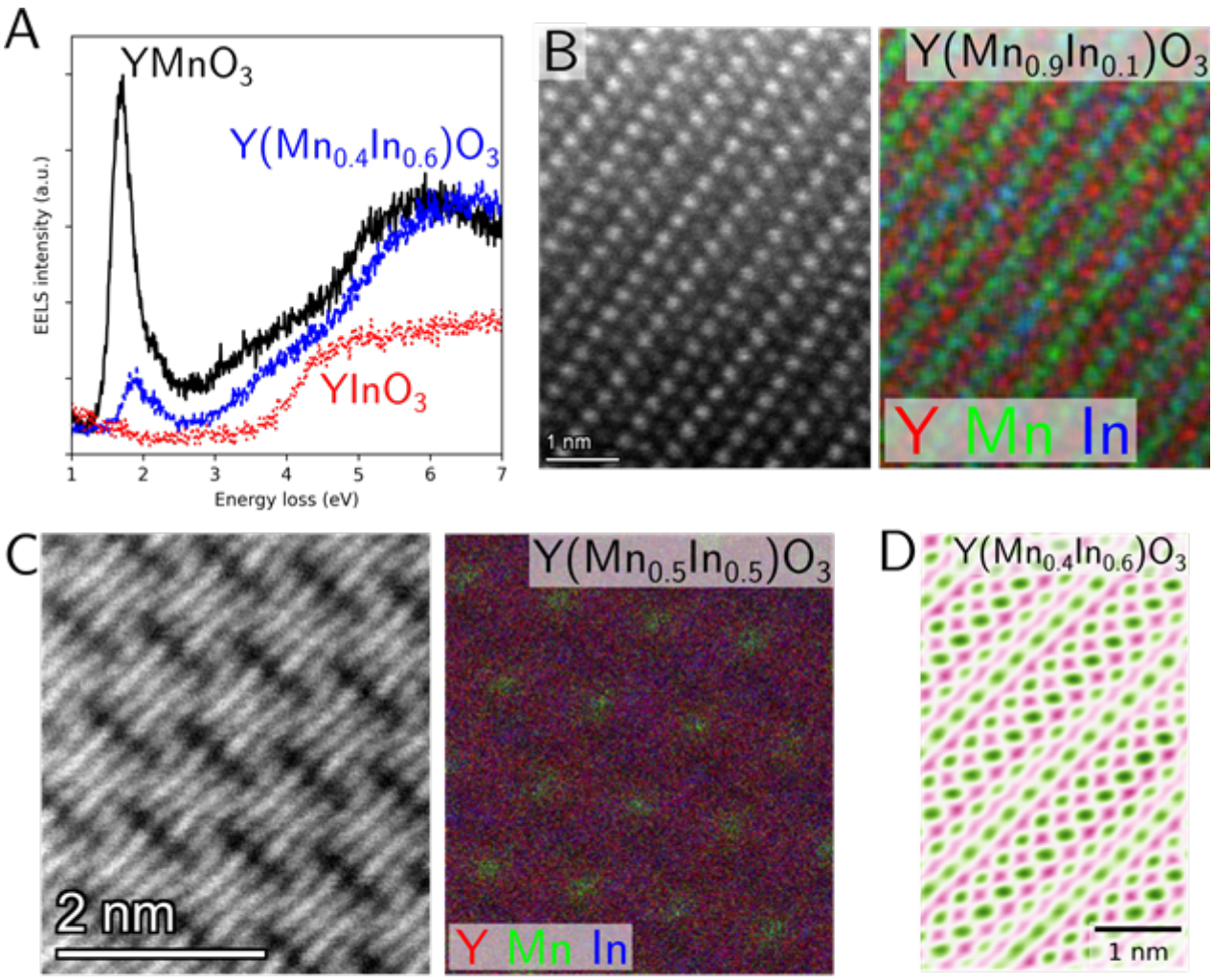

Fig. 1 A: Low-loss EELS spectra of three representative compounds spanning the compositional range. B: HR-STEM (left) and EDS (right) mapping of $Y(Mn_{0.9}In_{0.1})O_3$ along the [1-100] zone axis. C: HR-STEM (left) and EDS (right) mapping showing separation of the Mn and In lattice sites. D: iDPC image of an intermediate compound along the [1-100] axis

Keywords:

Oxide, optical, HR-STEM, HR-EELS

Reference:

[1] Subramanian and Li, Materials Today Advances, 16, 2022.
[2] Smith, et al., J. Am. Chem. Soc., 131, 47, 2009.
[3] Mukherjee, et al., Inorg. Chem., 57, 15, 2018.

669

Phase formation pathways of Me2+ oxides on sapphire (α-Al2O3) substrates

M.Sc. Yasemin Akyol[1], Dr. Sorour Semsari Parapari[2], Prof. Sašo Šturm[2], Prof. Cleva W. Ow-Yang[1,3], Prof. Mehmet Ali Gulgun[1,3]
[1]Materials Science and Nano Engineering, Sabanci University, Tuzla, Istanbul, Turkey, [2]Department for Nanostructured Materials, Jožef Stefan Institute, Jamova Cesta 39, Ljubljana, Slovenia, [3]Sabanci University Nanotechnology Application Center (SUNUM), Tuzla, Istanbul, Turkey

PS-09, Lecture Theater 2, august 26, 2024, 14:00 - 16:00

Background
Aluminate structures present phase formation anomalies irrespective of the initial stoichiometry of the oxide powder mixes. In metal oxide systems (Me2+ or Me3+), multiphases form at different cation to aluminum (Mex+/Al) ratios. Singh and his colleagues observed multiple phase formation in starting mixture ratios of CaO to Al2O3; 1:1, 1:2 and 3:1. Even if the stoichiometry started from calcium or aluminum rich compositions, CA was present in the diffractograms (Singh et al. 1990. p.873). Previous studies on calcium aluminates suggested that large cation size of Ca2+ may create a difficulty of diffusion into the Al2O3 (Tian et al. 2016. p.104). Tian and his coworkers demonstrated the distribution of Ca-rich phases with backscattered electron (BSE) images towards the outer layers of the core shell structure. In the center of this core shell structure Al2O3/CA6 was present. We observed that the first forming phase in strontium, calcium and yttrium aluminate systems is 1:1 oxide compound SA (SrAl2O4), CA (CaAl2O4), and YAP (YAlO3) irrespective of the starting Mex+/Al3+. This study claims that the Mex+/Al ratio at the interface determines the first forming incipient phase. Also, it appeared that having a single type of Al-O coordination polyhedra is facilitating the phase formation in aluminate systems.

Methods
SrO-Al2O3 binary system have 6 compounds: Sr4Al2O7, Sr3Al2O6, SrAl2O4, Sr4Al14O25, SrAl4O7, and SrAl12O19 (Fig.1). Phase pure aluminate powders were synthesized using Pechini method. Crystallization temperatures of aluminate powders were determined with thermogravimetric analysis. Phase distribution above 800-900 °C, the first crystallization, was recorded with ex-situ XRD by 50-100 °C temperature slots. Isothermal heating of 1 hour was applied to compounds. The temperature was increased until there was no change in the phase distribution of each compound. These powders were used to acquire Al-L2,3 and O-K ELNES edges of phase pure aluminate compounds with different stoichiometry to be used as a fingerprint of the compound.
Heating temperatures of deposited substrates were selected for each compound in a way that samples were XRD phase pure of desired stoichiometry. Amorphous or crystalline precursors having different Ca/Al ratio were deposited on sapphire substrates with different orientations. The effect of changing stoichiometry at the interface of the reaction couple was adjusted as a coating. Each deposited substrate was characterized with scanning electron microscopy (SEM) and X-Ray diffractometry (XRD) before the sample preparation for transmission electron microscopy (TEM). Then, the first structure to form at the interface was analyzed with the help of high-resolution TEM (HRTEM), HR-STEM, and EELS-ELNES. Different aluminate compounds at the interphase between reaction couples were compared with ELNES fingerprint of each pure aluminate compound.

Results
All sapphire substrates were analyzed with X-ray diffractometry (XRD). Four strontium aluminates were identified with ELNES edges (Fig.2 a-d). Al-L2,3 edge at an energy of 73.1 eV was chosen as the fingerprint for each aluminate compound. K edge of oxygen is at 532.0 eV. We tried to identify the

incipient structures at the interface of sapphire-aluminate film with different Sr2+/Al3+ ratio with the Al-L and O-K fingerprints of phase pure compounds.

Conclusion

Our study was a first attempt to clarify what kinetic constraints are determining the incipient metastable aluminate phase in Sr-, Ca-, Y- aluminate systems.

Graphic

Figure 1: Equilibrium binary phase diagram of SrO-Al2O3 (Van der Heggen, D. et al. 2022. p.3).

Figure 2. Al L2,3 ELNES edges of a) Sr4Al14O25 (S4A7), b) SrAl12O19 (SA6), c) SrAl4O7 (SA2) and d) Sr3Al2O6 (S3A), respectively.

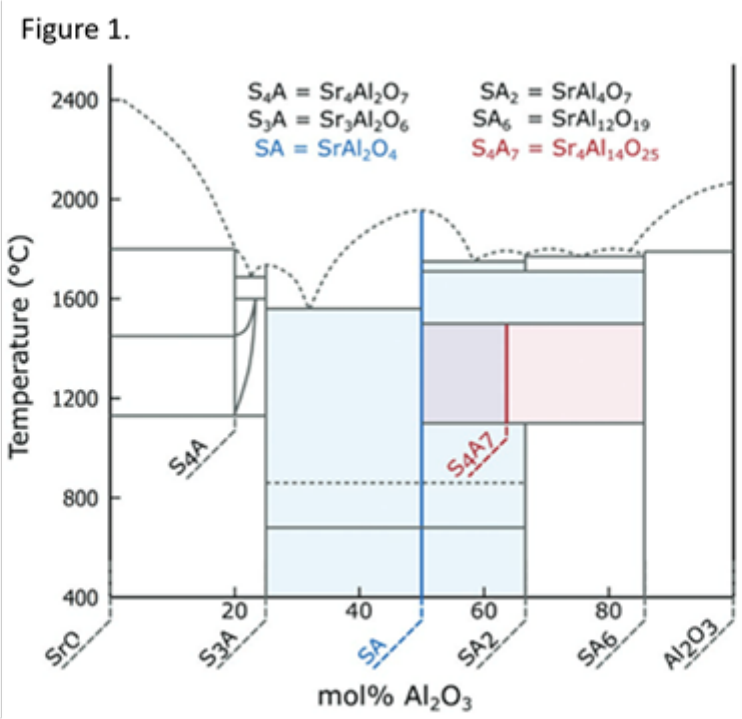

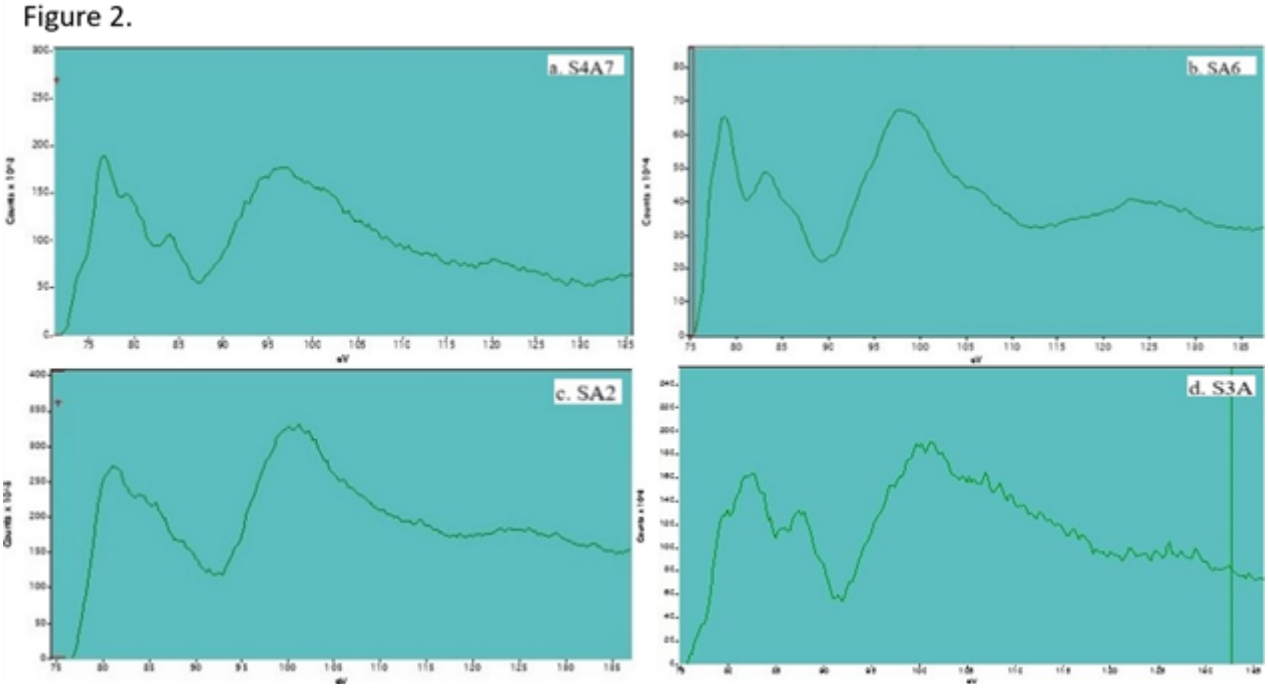

Keywords:

Interface reactions, aluminates, interphase, EELS

Reference:

1. Singh, V.K. Ali, M.M. Mandal, U.K. 1990. “Formation kinetics of calcium aluminates.” J Am. Ceram. Soc., 73, 872-876.
2. Tian, Y. Pan, X. Yu, H. Tu, G. 2016. “Formation mechanism of calcium aluminate compounds based on high-temperature solid-state reaction.” Journal of Alloys and Compounds, 670, 96-104.
3. Van der Heggen, D. Joos, J.J. Feng, A. Fritz, V. Delgado, T. Gartmann, N. Walfort, B. Rytz, D. Hagemann, H. Poelman, D. Viana, B. Smet, P.F. 2022. “Persistent luminescence in strontium aluminate: a roadmap to a brighter future.” AFM, 32: 1-31.
4. Retrieved on April 1, 2024, from: https://eels.info/atlas.

712

Oxygen vacancy imaging in complex oxides by a 4D-STEM optimized virtual detector

Francisco Fernandez Canizares[1,2], PhD. Student Isabel Tenreiro[1], Dr. Hamish Brown[3], Dr. Juan Ignacio Beltran Finez[1], Prof. Alberto Rivera Calzada[1], Prof. Maria Varela[1,2], Dr. Gabriel Sanchez-Santolino[1,2]
[1]Department of Materials Physics, Universidad Complutense de Madrid, Madrid, Spain, [2]Instituto Pluridisciplinar, Universidad Complutense de Madrid, Madrid, Spain, [3]Ian Holmes Imaging Center | Bio21 Molecular Science & Biotechnology Institute, Parkville, Australia

PS-09, Lecture Theater 2, august 26, 2024, 14:00 - 16:00

Background incl. aims
The interactions between the spin, charge, orbital and lattice degrees of freedom in transition metal oxides (TMO) give rise to a wide range of emergent phenomena, such as high temperature superconductivity, colossal magnetoresistance, or metal-insulator transitions, to name a few. Small variations in local chemical or electronic doping resulting from the presence of O vacancies can lead to drastic changes in these physical properties, since the macroscopic response is ultimately determined by the interplay between the oxygen s-like and transition metal d-like electrons. Thus, the in-depth comprehension of such phenomena relies on being able to quantify the presence of very reduced densities of these elusive defects. However, the detection of very low O vacancy concentrations remains extremely challenging. Aberration-corrected electron probes in the scanning transmission electron microscope (STEM) can bear on this task. In this work we propose a new method aimed to detect single O vacancies in a TMO such as SrTiO3 (STO), exploiting the capabilities of 4D-STEM techniques.
Methods
Density-functional theory (DFT) calculations were used to obtain reference relaxed STO supercells containing a single oxygen vacancy per 3x3x9 unit cells in order to mimic very low deoxygenation levels. Simulations of 4D-STEM data based on these models were carried out using the py_multislice code. Convergent beam electron diffraction (CBED) patterns of fully oxygenated O columns and columns with a single oxygen vacancy were obtained. Simulations have been performed implementing the multislice method in combination with the frozen phonon approximation, to account for multiple and thermal diffuse scattering. Analysis of the scattered intensity distribution, as a function of scattering angle and specimen thickness, allows identification of the characteristic fingerprints associated with the presence of single oxygen vacancies in atomic resolution diffraction images. A virtual detector can be used post-acquisition to generate images from 4D-STEM datasets. The imaging geometry was optimized here by selectively picking a distribution of inner/outer angles of annular detectors. Angular ranges were chosen to maximize intensity variations when comparing individual O atomic columns, and a virtual imaging mode was engineered to maximize the contrast between fully oxygenated columns and atomic columns where single O vacancies were present. Such simulations were then used for comparison with experimental 4D-STEM data obtained from ultrathin, freestanding SrTiO3 membranes 16 nm thick with O vacancy concentrations bellow the sensitivity threshold of complementary techniques such as electron energy-loss spectroscopy (EELS).
Results
The contribution to the electron scattered intensity distribution associated with O columns where a single oxygen vacancy is located can be quantified by subtracting the CBED pattern from a fully oxygenated column to a vacancy containing column, as illustrated in Fig. 1. The analysis of the resulting scattered intensity distribution reveals two angular regions of interest: (1) a central region inside the bright field disk where fully oxygenated columns scatter in a more intense fashion due to beam channeling and (2) an external region in the bright field disk where the scattering intensity is increased due to a dechanneling effect. This behavior is robust and easily interpretable upon sample

thickness variations. Such well-defined angular dependence of the scattered intensity constitutes a characteristic fingerprint of single oxygen vacancies.
Experimental data can be then examined with these features in mind. Experimental 4D-STEM datasets were analyzed using the virtual detector previously discussed in order to track spatially any O column intensity variation. Optimized detector images were produced by integrating the relevant angular ranges in experimental data. The resulting images exhibit, indeed, variations in O column intensity that are consistent with small amounts of O vacancies, which can be identified well above the noise threshold. Results will be shown to prove that both image contrast difference and single CBED pattern features demonstrate single vacancy detectability. The contrast difference between fully oxygenated and vacancy containing columns in the optimized virtual detector imaging mode will also be discussed in the light of conventional annular dark field (ADF) and annular bright field (ABF) images.
Conclusion
We demonstrate the detection of single oxygen vacancies in SrTiO3. Combining DFT calculations, atomic resolution 4D-STEM simulations and data analysis, the characteristic fingerprints of single oxygen vacancies can be identified in both simulations and experimental data, which indeed replicate the predicted fingerprints both in image intensity and CBED patterns. This capability enables for the first time the experimental identification of single oxygen vacancy columns in a freestanding STO membrane. This method opens a new path in the field of advanced materials characterization by electron probes, highlighting the advantages of 4D-STEM techniques and the unique insight they provide.

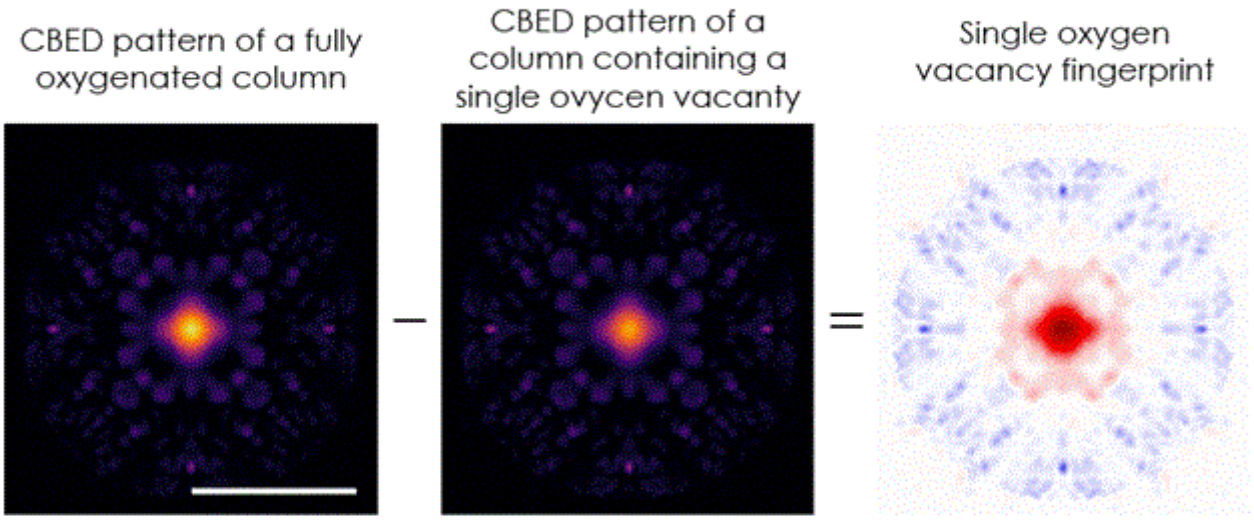

Figure 1. Scattered intensity distribution study. Simulated CBED patterns obtained from fully oxygenated and columns containing a single oxygen vacancy are subtracted to extract the contribution to the scattered intensity distribution of a single oxygen vacancy. Two regions of interest are revealed: (1) internal region of the bright field where fully oxygenated columns scatter greater intensity (in red) and (2) external region of the bright field where the scattering from vacancy columns is more intense (blue). Simulation correspond to a 200 keV beam with a probe forming semi-angle of 30 mrad in surface focus condition, for a single oxygen vacancy situated 4-unit cells bellow the surface and a sample thickness of 16 nm. The Scale bar corresponds to 30 mrad. Column CBED signal scale spans the 0 to 0.15 % of the incident intensity range. Fingerprint intensity scale corresponds to -0.02 % to 0.02 % of incident intensity.

Keywords:

4D-STEM, oxygen-vacancies, complex-oxides, vacancy ordering

Reference:

[1] Hwang, H. Y. et al. Emergent phenomena at oxide interfaces. Nat Mater 11, 103–113 (2012).
[2] Varela, M. et al. Atomic-resolution imaging of oxidation states in manganites. Phys Rev B 79, 1–14 (2009).
[3] Ophus, C. Four-Dimensional Scanning Transmission Electron Microscopy (4D-STEM): From Scanning Nanodiffraction to Ptychography and Beyond. Microscopy and Microanalysis 25, 563–582 (2019).

[4] Ooe, K.,Seki, T., Ikuhara, Y. & Shibata, N. Ultra-high contrast STEM imaging for segmented/pixelated detectors by maximizing the signal-to-noise-ratio. Ultramicroscopy 220, 113133 (2021).
[5] Brown, H. G., Pelz, P., Ophus, C. & Ciston, J. A Python Based Open-source Multislice Simulation Package for Transmission Electron Microscopy. Microscopy and Microanalysis 26, 2954–2956 (2020).

1168

Mapping the Space Charge Region in BaTiO3 and SrTiO3 using 4-Dimensional Scanning Transmission Electron Microscopy

Dr Sangjun Kang[1], Dr Di Wang[2], Dr Dylan Jennings[3], Prof Wolfgang Rheinheimer[4], Prof Christian Kübel[1], Prof Xiaoke Mu[5]
[1]Tu Darmstadt, Darmstadt, Germany, [2]Karlsruhe Institute of Technology , Karlsruhe , Germany, [3]Forschungszentrum Jülich GmbH, Jülich, Germany, [4]University of Stuttgart, Stuttgart, Germany, [5]Lanzhou University, Lanzhou, China

PS-09, Lecture Theater 2, august 26, 2024, 14:00 - 16:00

Ceramic capacitors are passive electronic components designed to store and release electrical energy through an electric field [1]. Polycrystalline barium titanate (BaTiO3) and strontium titanate (SrTiO3) have been widely employed in ceramic capacitors due to their reliable dielectric properties, compact size, and cost-effectiveness [2]. However, this material experiences degradation, such as increased leakage current, as a result of diminishing resistance under elevated temperatures and voltage stress. According to the ionic de-mixing model, the primary cause of this degradation is the migration of oxygen vacancies, which move toward grain boundaries and eventually reach the cathode [3].
The migration of oxygen vacancies can be effectively altered by doping with elements such as Fe and Mn. This doping modifies the Fermi level and the space charge region (SCR) at grain boundaries. The SCR is the result of an accumulation or depletion of oxygen vacancies and cations around grain boundaries, limiting their migration and preventing degradation. However, this general description lacks validation of the details such as the influence of grain boundary character on the SCR due to limited microscopic observations of grain boundaries and SCR in ceramic capacitors, making it challenging to further develop the theory.

In this study, we employ 4-dimensional scanning transmission electron microscopy (4D-STEM) [4] in combination with electron precession to map electric fields at grain boundaries in Fe-doped BaTiO3 and SrTiO3. Unlike conventional differential phase contrast (DPC) analysis, electric field mapping by 4D-STEM reduces diffraction and channeling artifacts thus enabling accurate measurement of electric field and charge density at the grain boundary. Combining it with an in-situ biasing TEM setup, we can visualize SCRs under different biasing conditions at various temperatures. Through our presentation, we aim to showcase our methodological developments and observations of SCRs in BaTiO3 and SrTiO3. These findings promise to significantly advance the fundamental scientific understanding of ceramic capacitor performance and illuminate the degradation mechanisms under high voltage stress.

Keywords:

Space Charge Layer, 4D-STEM

Reference:

[1] K. Hong, T. H. Lee, J. M. Suh, S.-H. Yoon, and H. W. Jang, “Perspectives and challenges in multilayer ceramic capacitors for next generation electronics,” Journal of Materials Chemistry C, vol. 7, no. 32, pp. 9782–9802, 2019.
[2] Vijatović, M. M., J. D. Bobić, and Biljana D. Stojanović. "History and challenges of barium titanate: Part II." Science of Sintering 40.3 (2008): 235-244.
[3] R. Giesecke, R. Hertwig, T. J. M. Bayer, C. A. Randall, and A. Klein, “Modification of the Schottky barrier height at the RuO2 cathode during resistance degradation of Fe-doped SrTiO3,” Journal of the American Ceramic Society, vol. 100, no. 10, pp. 4590–4601, 2017.

[4] Kang, Sangjun, et al. "Direct observation of quadrupolar strain fields forming a shear band in metallic glasses." Advanced Materials 35.25 (2023): 2212086.

20

The behavior of additive manufactured aluminum alloys upon anodization

Lydia Daum[1], Dr. Stefan Ostendorp[1], Dr. Martin Peterlechner[2], Prof. Dr. Gerhard Wilde[1]
[1]Institute of Materials Physics, University of Münster, Münster, Germany, [2]Laboratory of Electron Microscopy, Karlsruhe Institute of Technology, Karlsruhe, Germany

Poster Group 1

Background incl. aims
Additive manufacturing of aluminum alloys, i.e. laser powder bed fusion (3D printing), introduces significant versatility and innovation to various industrial applications. Al-Fe-Zr alloys, which are suitable for additive manufacturing, exhibit mechanical properties comparable to conventionally cast aluminum alloys that are alloyed with Mg, Mn and Si, such as the 60xx series Al-alloys. Anodization of aluminum alloys is performed to enhance their chemical and mechanical performance by the formation of a protective anodic aluminum oxide (AAO) layer. The absence of those 60xx series alloying elements in Al-Zr-Fe, which typically form voids in AAOs and alter the structural integrity, suggest a distinct anodization behavior. This might lead to improved chemical and mechanical properties of the grown passivation layer.
Additionally, the overall microstructure of 3D printed alloys inherently differs from conventionally casted, processed and artificially aged microstructures of the same alloy. Here, a variety of elongated and equiaxed grains are observable along the printing direction. This disparity underscores the necessity for a comprehensive comparison of differently treated microstructures prior to anodization. Afterwards, the anodization behavior of Zr- and Fe-enriched precipitates are investigated to ascertain their impact on the chemical resistivity of the resulting AAOs.
Methods
The microstructure of the Al-Fe-Zr alloy was modified through changes in the manufacturing method, varying degrees of severe plastic deformation and adjustments to the heat treatment before anodization. Polished sample surfaces are analyzed with EBSD and subsequently anodized under galvanostatic conditions in oxalic acid solutions following a standardized protocol which allows to determine the impact of different precipitates' sizes and electrochemical potentials. All AAO-coated samples are bisected using a wire saw, which each half treated independently thereafter. The first half is directly coated with Cr/Au to enhance electron conductivity for TEM lamella preparation in FIB whereas the other half was exposed to reactive ion etching to study the chemical resistivity of the AAO.
TEM samples are prepared by employing Ga-, Si/Au- or He/Ne-FIB on randomized surface positions. The AAOs were analyzed in a Gatan Double Tilt LN2 Cooling Holder 636 using a Titan Themis 60 – 300 operated at 300 kV and at a temperature of 96 K. EDX spectra are recorded with a quadrupole SuperXG2 detector. A CCD-GIF camera is used to record nano-beam diffraction patterns (NBDPs), also denoted as 4D-STEM. Beam damage is suppressed by using beam currents as low as 10 pA during NBDP acquisition.
Results
Given the difference of current densities during anodization of various types of microstructures while maintaining the standardized protocol, the analysis of various NBDPs of different precipitates – each with a stack size of at least 10000 NBDPs – suggests a size-dependent anodization behavior of Fe-enriched precipitates and underscores the influence of the underlying microstructure and the participating precipitates on the grown AAO thickness. Using 4D-STEM and fluctuation electron microscopy, various oxide types within the AAO were distinguished and information about the precipitates' structure and chemistry are correlated, which supports the hypothesis of size- and type dependent influence. Ga-contamination due to FIB preparation at grain and phase boundaries was

diminished by changing to Si/Au or He/Ne FIB for the final polishing step. Finally, we attribute the microscopic differences in AAO growth to macroscopic properties such as chemical resistivity.
Conclusions
Based on the results, Fe-rich precipitates remain partially unaffected by anodization, depending on their size and type, while Zr-rich ones are anodized with the matrix. Unlike conventional alloys, Al-Zr-Fe alloys do not develop voids within the AAO, which leads to a distinct chemical resistivity. Moreover, the microstructure is affecting the properties of the AAO. This emphasizes the importance of selecting an advantageous microstructure tailored to the intended application of the protective layer.

Keywords:

Anodization, 4D-STEM, cryogenic measurements, precipitates

104

Mapping Orthorhombic Domains with Geometrical Phase Analysis

Bernat Mundet[1], Mr. Marios Hadjimichael[2], Jennifer Fowlie[3], Lukas Korosec[4], Lucia Varbaro[4], Claribel Domínguez[4], Prof. Jean-Marc Triscone[4], Duncan Alexander
[1]Catalan Institute of Nanoscience and Nanotechnology (ICN2), Bellaterra, Spain, [2]Department of Physics, University of Warwick, Warwick, United Kingdom, [3]Stanford University, Stanford, USA, [4]Department of Quantum Matter Physics, University of Geneva, Geneva, Switzerland, [5]Electron Spectrometry and Microscopy Laboratory (LSME), Institute of Physics (IPHYS), École Polytechnique Fédérale de Lausanne ole Polytechnique Federal de Lausanne (EPFL), Lausanne, Switzerland

Poster Group 1

Background incl. aims

Perovskite oxide compounds, with the chemical formula ABO3, constitute one of the most studied family of oxides due to its large variety of fascinating properties combined with their high degree of tunability. Although the prototypical perovskite lattice is cubic, additional structural distortions emerge when the ionic size ratio (A/B) deviates from one, thus lowering its symmetry. Among all the possible resulting space groups, the orthorhombic Pbnm lattice is one of the most common ones. For instance, most Vanadates, Nickelates, Iridates and Titanates share these particular lattice symmetries. The anisotropic unit cell of such compounds is characterized by in-phase octahedral rotations about one pseudocubic axis (the long orthorhombic one) and out-of-phase rotations about the other two pseudocubic ones; plus additional relative A-site displacements that feature a zig-zag pattern along the [110]PC direction.
When growing epitaxial heterostructures, the Pbnm lattice may nucleate differently oriented depending on how the unit cell is constrained by its neighboring epitaxial layers. When different orientations are equally energetically favorable, the presence of lattice domains with distinct orientations emerge, which in turn may lead to the presence of crystal defects. Retrieving all of this information is therefore paramount when designing novel heterostructures for electronic devices, as it will affect their resulting physical properties. For instance, improper ferroelectricity in artificial superlattices requires the long orthorhombic axis to be oriented out-of-plane. However, since the three pseudocubic axes are in most of the cases very similar in length, it is typically challenging to extract this information from conventional X-ray diffraction analyses.

Methods

In this contribution, we present a very simple and fast approach devoted to map Pbnm lattice domains.1 It is based on using the conventional geometrical phase analysis (GPA) but in a non-conventional manner. Since the relative zig-zag displacements of the A-site cations double the unit cell length along the long orthorhombic axis, they feature additional half-order reflections in the Fourier Transform (FT) pattern of aberration-corrected STEM images. The strategy behind our methodology consists then on using the conventional aperture settings used for regular strain mapping (centered in the (001)PC and (100)PC or (010)PC reflections), but this time including the {(1/2) 0 1}PC or {1 0 (1/2)}PC reflections within the selected aperture area as well. When these particular aperture settings are used, additional fringes (related to the A-site relative displacements) appear in the exy and rxy maps only in those areas contributing to the emergence of these half-order reflections in the corresponding FT pattern.

Results

As a showcase of the versatility and robustness of this methodology, we further exploit this approach to determine the structural parameters that set the lattice orientation and associated domain distribution in rare-earth nickelate compounds. For this, we have analyze the domain distribution in a

series of rare-earth nickelate heterostructures grown under distinct structural constraints. Although we will show that the resulting lattice orientation and domain distribution mainly depends on the in-plane normal epitaxial strain, we will also demonstrate how shear strain and interfacial structural connectivity are also very relevant, and should not be neglected when designing novel heterostructures.1-3
Finally, we will also show that this methodology is not restricted to Pbnm domain mapping, but can also be exploited to identify some specific lattice defects or domain boundaries that are otherwise very challenging to localize. Further, beyond Pbnm compounds, it can be adapted to map other types of structural periodicities from other space groups that also also render half-integer reflections in the FT patterns of STEM images.

Conclusion
To summarize, in this contribution we will first present a fast, robust and versatile methodology that is very useful to map Pbnm lattice domains. Second, we will discuss how we have applied this to identify key structural parameters that influence domain distributions in epitaxially-grown Pbnm compounds. Finally, we will also comment about other possible scenarios where this methodology can be also useful to track and map periodic structural distortions that render half-integer reflections in the FT patterns of STEM images.

Keywords:

STEM, GPA, Perovskites, strain, mapping.

Reference:

1 B. Mundet, H. Hadjimichael et al., APL Materials 12, 031124 2024
2 L. Varbaro, B. Mundet et al., APL Materials 12, 031104 (2024)
3 D. Alexander, H. Meley, et al., arXiv : 2401.08798v1

217

In situ observation of dislocation evolution in cerium oxides nanocubes in an environmental TEM

Dr Lucile Joly-Pottuz[1], Dr Rongrong Zhang[1], Dr Thierry Epicier[2], Dr Gaetan Laurens[3], Dr Tristan Albaret[3], Pr Karine Masenelli-Varlot[1]
[1]MATEIS - INSA, , France, [2]IRCELYON - UCBL, , France, [3]ILM - UCBL, , France

Poster Group 1

Characterizing the mechanical properties and deformation mechanism of ceramic materials at the nanoscale is of much interest to improve their processing and properties. At the nanoscale, plastic deformation have already been observed in alumina and magnesium oxide nanoparticles at room temperature. Cerium oxide, as one of the most important ceramic materials, is widely used in many applications, such as in solid oxide fuel cell electrodes, catalysis, or gas detection. However, there are few experimental pieces of evidence of the evolution of defects, which have significant impact on many material properties, especially on mechanical behavior. TEM observations of CeO2 nanocubes demonstrated a beam sensitivity with reduction under high electron dose. Reduction may have an impact on the mechanical properties. The development of TEM nanocompression experiments inside an environmental transmission electron microscope (ETEM) is of much interest to study the mechanical properties of ceramic particles and the effect of the reduction on them. High resolution imaging may also be very useful to fully study the defects formation (dislocations, stacking faults…) during compression. In situ nanocompression under gas and at high resolution in an ETEM were developed on CeO2 and are reported in this work.

Cerium oxides nanocubes (20-50nm size) were compressed using a dedicated Hysitron PI 95 sample holder in an environmental transmission electron microscope (ETEM). By controlling the electron dose and by using a small pressure of air in the ETEM, different CeOx structures (x between 1.5 and 2) were tested to compare their mechanical properties and their deformation mechanisms. Displacement-controlled in situ compression tests were performed in a Titan ETEM 80-300 kV microscope equipped with a Bruker PI95 picoindenter. The loading direction was [100]. Different imaging techniques have been used to identify the slip systems in CeO2. High resolution imaging has also been performed during compression of Ce2O3 nanocubes to observe dislocations, stacking fault or nano-twin formation. Simulation calculations (DFT, DM) are very useful to complete/understand the in situ nanocompression experiments and were developed on CeOx material, even if computing time might be long due to the complexity of the structures

.

CeO2 has a fluorite structure (space group Fm-3m). Their reduction under the electron beam creates oxygen vacancies in the structure, which leads to a fcc bixbyite structure (space group Ia-3) with a double cell parameter compared to fluorite. In the case of CeO2, deformation mechanism is found to be similar to those observed in other fluorite structure, with <110> {111} slip systems. The evolution of the yield stress with the nanocube size reveals to be similar to the one already observed for other fcc structures. In the case of Ce2O3 bixbyite structure few studies have reported the deformation mechanism and the slip systems so far. Oxygen vacancies may play a role in defect formation. To observe the deformation mechanisms accurately, high resolution imaging could be performed during in situ nanocompression. Dissociation of perfect dislocations into partials and stacking faults has been observed, which is unusual in oxides. The results obtained for both structures are discussed and compared to simulations works. Compression cycles carried out on the same nanocube under different irradiation conditions (thus either in the fluorite or in the bixbyite structure) will be shown to highlight the differences between both mechanisms.

.

In situ nanocompression experiments have been used to study and compare the deformation mechanism of CeOx nanocubes. On single nanocubes, different mechanisms have been evidenced depending on the irradiation conditions and thus the crystallographic phase. When compressed along the <100> direction, fluorite deforms at room temperature via <110> {111} perfect dislocations and the effect of the nanocube size on the yield stress is similar to what is observed in other fcc materials. In bixbyite, the dislocations dissociate and form stacking faults. This process is reversible.

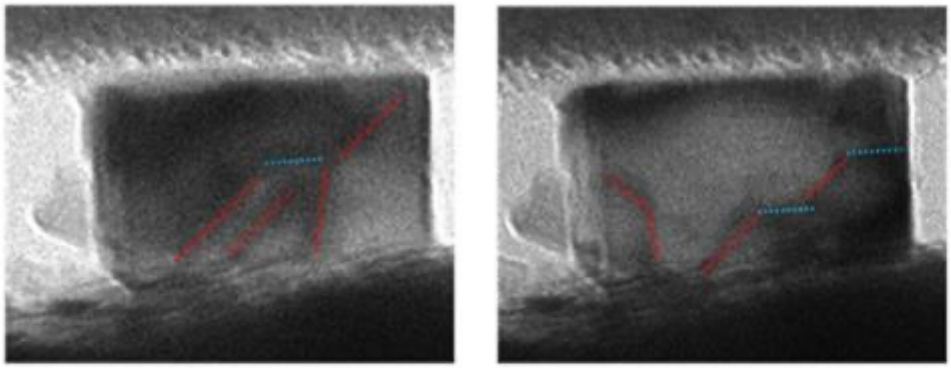

½[101](10-1) ½[01-1](111) ½[011](1-11) ½[10-1](1-11)

Keywords:

In-situ
Nanocompression
ETEM
Oxides

362

Transformation of Al2O3 to Cr-rich spinel during spark plasma sintering of alumina dispersed 316L steel

Dr. Zsolt Czigány[1], Dr. Haroune Rachid Ben Zine[1,2], Dr. Csaba Balázsi[1], Dr. Katalin Balázsi[1]
[1]Institute of Technical Physics and Materials Science, HUN-REN Center for Energy Research, Budapest, Hungary, [2]Faculty of Sciences and Technology, Mohamed Khider University, Biskra, Algeria

Poster Group 1

Background incl. aims
Dispersion of oxide particles in sintered steels is generally applied to improve the mechanical properties (e.g. fracture toughness, creep resistance) of steels. Spark plasma sintering (SPS) is a relatively new method [1] when a sequence of electric pulses are applied at high temperature and pressure. As an advantage, SPS offers rapid heating, limitation of grain growth, and efficient densification kinetics, which may provide benefits over hot isostatic pressing in certain applications. Manufacturing by SPS can also provide significant savings by increasing production volume and reducing energy costs.
Methods
Oxide dispersion strengthened (ODS) 316L stainless steel alloys with dispersed alumina were prepared by attrition milling and spark plasma sintering process at 900°C. The location and crystal structure of the oxide phase was investigated by a Cs corrected Themis (Thermo Fisher) transmission electron microscope including HRTEM, SAED [2] and EDS elemental mapping. TEM specimens were prepared by Ar ion beam milling at incidence angle of 4° at 10kV using a Technoorg Linda equipment [3]. The thinning procedure was finished at low-energy of 300 eV in order to minimize the possible ion beam damage.
Results
During sintering, the dispersed alumina transformed to spinel phase, dominantly with Cr2AlO4 composition. The spinel crystallites were observed between the grains of stainless steel in the sintered composites. The spinel crystallites were surrounded by an amorphous silica phase. The necessary Cr and Si may segregate from the stainless steel alloy at SPS conditions. The lattice parameter of the formed spinel phase is 8.36Å independent of the local composition variation as indicated by FFT of high resolution images.
Conclusions
The lattice parameter of the spinel phase is close to the high end among chromite related spinels which implies that octahedral sites of spinel structure are mainly occupied by Cr3+ or possibly Fe3+ cations [4]. These findings are consistent with literature describing geological formation of spinels in mafic or ultramafic rocks with low oxygen fugacity and assistance of silica phase in cation exchange [5].

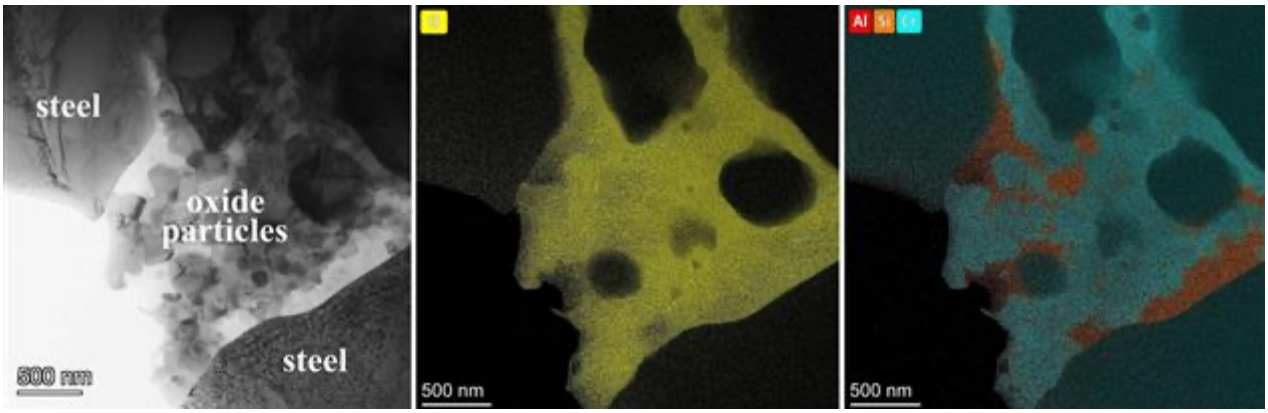

Keywords:

Keywords:
spinel, cation exchange, sintering

Reference:

[1] Cs. Balázsi, F. Gillemot, M. Horváth, F. Wéber, K. Balázsi, F. Cinar Sahin, Y. Onüralp, and Á. Horváth Preparation and structural investigation of nanostructured oxide dispersed strengthened steels. J Mater Sci 46 (2011) 4598–4605
[2] Zsolt Czigány and Viktória Kovács Kis Acquisition and evaluation procedure to improve the accuracy of SAED. Microscopy Research and Technique 86 (2023) 111870
[3] Á. Barna, "Topographic kinetics and practice of low angle ion beam thinning," Materials Research Society Symp. Proc. 254 (1992) 3
[4] Davide Lenaz and Henrik Skogby, Structural changes in the FeAl2O4–FeCr2O4 solid solution series and their consequences on natural Cr-bearing spinels, Phys Chem Minerals 40 (2013) 587–595
[5] S.J. Barnes, P.L. Roeder: The range of Spinel Compositions in terrestrial Mafic and Ultramafic Rocks Journal of Petrology 42 (2001) 2279-2302

782

Hybrid electrospun scaffolds for enhanced collagen formation in regeneration processes: electron and confocal microscopy analysis

Dr Joanna Karbowniczek[1], Dr Krzysztof Berniak[1], Prof. Urszula Stachewicz[1]
[1]Faculty of Metals Engineering and Industrial Computer Science, AGH University of Krakow, Krakow, Poland

Poster Group 1

Background

Extracellular matrix (ECM) of bone tissue is a natural composite containing organic and inorganic components, that can be biomimicked using electrospun fibers. Addition of ceramic filler into the polymer fibers can enhance the mechanical properties as well as improve bioactivity. However, to obtain the best hybrid scaffold the uniform distribution of particles and reduction of aggregations are necessary [1]. Here, the careful design of composite fibers can trigger cellular adhesion, proliferation and tissue regeneration via enhance collagen formation in the in vitro cell culture [2]. Therefore, the goal of this work is to optimize and verified production of hybrid electrospun fibers for effective bone tissue scaffolds including visualization using advance electron and confocal microscopy analysis.

Methods

Blend and co-axial electrospinning were employed to manufacture bone scaffolds of poly(3-hydroxybutyrate-co-3-hydroxyvalerate) (PHBV) with incorporated titanium dioxide nanoparticles (TiO_2) using TechNOVA electrospinning device [3]. Morphology of obtained fibers was evaluated by scanning electron microscopy (SEM) with secondary electron detector (Merlin, Zeiss). Distribution and aggregation of TiO_2 within polymer fibers were studied by SEM imaging with back scattered detector (BSE), energy dispersive X-Ray spectroscopy (EDS, detector Brucker). Additionally similar analysis was also performed at the cross-sections prepared by focused ion beam (FIB, Crossbeam 350, Zeiss). In vitro cell culture study was performed with osteoblast cells up to 14 days. Cell proliferation and morphology in response to various scaffolds was verified after 1, 3 and 7 days of incubation. The collagen formation was confirmed by immunofluorescence staining and visualized by confocal laser scanning microscopy (CLSM, LSM 900, Zeiss).

Results

Over 20% increase in fiber diameter was observed when PHBV was enriched with TiO_2 nanoparticles, reaching 3.84 µm for sample prepared by co-axial process. Blend fibers had smooth surface with visible large particles aggregations, locally exceeding 5 μm^2, in majority covered by polymer. On the other hand, the fibers prepared using co-axial nozzle had core-shell morphology, with polymer fibers homogenously decorated with ceramic particles with significantly smaller aggregations up to 0.3 μm^2. In response to core-shell fibers cells exhibited significantly higher proliferation after 7 days with excellent spreading within the scaffold structure. Additionally, they produced vast network of collagen fibers as the important stage of ECM formation, which was not observed in such extent for any other tested scaffold.

Conclusion

Current study shows the importance of electrospinning strategy for single-step production of bioactive scaffolds supporting bone regeneration. For cellular guidance it is essential not only to provide composite morphology but also to ensure proper particles distribution and availability, which was achieved by co-axial electrospinning. The presence of ceramic nanoparticles, effectively integrated onto the surface of polymer fibers, enhances cells adhesion, ingrowth and promotes the formation of ECM, which are necessary in tissue regeneration processes.

Acknowledgements
This study was financially supported by OPUS 17 project granted by the National Science Centre, Poland No 2019/33/B/ST5/01311 and by PIECRISCI project founded by the European Union's Horizon 2020 research and innovation programme under grant agreement No 958174 and within M-ERA.NET 3 funded by National Science Centre, Poland No 2021/03/Y/ST5/00231.

Keywords:

Organic-inorganic composites, bone, collagen staining

Reference:

[1] J.E. Karbowniczek et al. Composites Part B 241 (2022) 110011, DOI: 10.1016/j.compositesb.2022.110011
[2] P.K. Szewczyk et al., Nanoscale, 2023, 15, 6890, DOI: 10.1039/d3nr00014a
[3] J.E. Karbowniczek et al., J. Colloid Sci. 650 (2023) 1371–1381, https://doi.org/10.1016/j.jcis.2023.07.066

790

Structural study of perovskite-structure transition metal oxide thin film using Cs-corrected STEM: case of $LaVO_3/DyScO_3$

Chih-ying Hsu[1,2], Clementine Thibault[1], Pau Torruella[2], Jean-Marc Triscone[1], Stefano Gariglio[1], Duncan T.L. Alexander[2]
[1]Department of Quantum Matter Physics, University of Geneva, Geneva, Switzerland, [2]Electron Spectrometry and Microscopy Laboratory (LSME), Institute of Phyiscs (IPHYS), École Polytechnique Fédérale de Lausanne (EPFL), Lausanne, Switzerland

Poster Group 1

Rare-earth transition metal perovskite oxides illustrate strong correlations between atomic structure and functional properties (1). When deposited as thin films, this enables manipulation of their electronic properties, for instance by tuning their composition or strain state. To understand these correlations, Cs-corrected scanning transmission electron microscopy (Cs-STEM) has become an important tool to measure the deposited lattices, not only to resolve and identify atomic columns, but also to locate their positions with a few picometer precision.
In this study, we focus on rare-earth vanadate films of composition $LaVO_3$ that are grown, at different temperatures, by pulsed laser deposition (PLD) on (110) $DyScO_3$ substrates. The epitaxial strain resulting from the lattice mismatch between the $DyScO_3$ substrate and $LaVO_3$ film is supposed to be around +0.5% (film under tension). However, in a series of thin films, a change in $LaVO_3$ unit cell volume is observed that depends on the deposition temperature. A double-corrected FEI/Thermo Fisher Scientific Titan Themis 60-300 is used to study the different samples in STEM mode, operated at 300 kV with beam currents down to 50 pA. STEM images are recorded as 90° rotation series, which are then processed using rigid and non-rigid alignment to maximize measurement precision (2). Both the film and the substrate adopt a Pbmn orthorhombic lattice. Depending on the TEM lamellae orientation, different characteristic orthorhombic distortions of the sample can be probed. Data treatment using the open-source python library Atomap (3) coupled with an in-house library allows measurements of the various distortions, i.e., oxygen octahedral rotations and A-site cation antipolar displacements.
Here, we investigate in depth how the different PLD growth parameters affect the $LaVO_3$ film structure. As suggested by X-ray diffraction measurements, key factors include growth temperature and O_2 partial pressure. With the Cs-STEM measurements, we are able to monitor their effects in real space. In particular, we have recently identified a novel structural organization in the $LaVO_3$ film called the “switching plane,” where the orthorhombic long axis direction switches 90° due to a competition between opposing energetic influences on the film’s orientation (4). We study the influence of growth temperature (and unit cell volume), and O_2 partial pressure on the switching plane formation and location, as characterized by spatially mapping the magnitude and direction of the orthorhombic distortions across the film thickness. Our latest results suggest that induced strain state and/or thermal energy play major roles in defining the presence of this novel structural formation.

Keywords:

Perovskite thin film, orthorhombic distortion

Reference:

1. J. H. Ngai, F. J. Walker, C. H. Ahn, Annual Review of Materials Research. 44, 1–17 (2014).
2. L. Jones et al., Advanced Structural and Chemical Imaging. 1, 8 (2015).

3. M. Nord, P. E. Vullum, I. MacLaren, T. Tybell, R. Holmestad, Advanced Structural and Chemical Imaging. 3, 9 (2017).
4. D. T. L. Alexander et al., Switching plane: A novel crystalline interface in orthorhombic perovskite films (2024), doi:10.48550/arXiv.2401.08798.

828

Detailed TEM Studies of 1D Nanostructures based on Layered Cobalt Oxide

Dr Raul Arenal[1,2,3], Dr Simon Hettler[1,2], Mrs Kankona Roy[4], Dr. Leela Panchakarla[4]
[1]Instituto de Nanociencia y Materiales de Aragón, CSIC-Universidad de Zaragoza, Zaragoza, Spain., Zaragoza, Spain, [2]Laboratorio de Microscopías Avanzadas, Universidad de Zaragoza. Zaragoza, Spain, Zaragoza, Spain, [3]Araid Foundation, Zaragoza, Spain, Zaragoza, Spain, [4]Department of Chemistry, Indian Institute of Technology Bombay, , Powai, Mumbai, 400076, India

Poster Group 1

Background incl. aims:
The oxide misfit layered compounds (MLC) are heterostructures with complex stacking usually formed by two ceramic oxide layers. These oxides exhibit remarkable structural and chemical complexity and show very interesting electronic, thermoelectric, and magnetic phenomena [1-5]. It is interesting to mention that due to the intrinsic asymmetry of MLCs, they tend to bend and shape into tubular structures in the form of 1D nanomaterials: nanotubes (NTs) and nano-scrolls (NS) [1-5]. There are two different synthesis routes of these nanomaterials, the starting material is either a mixture of the individual constitutive elements or directly is the corresponding bulk structure. Following the latter pathway, recently, we have developed novel synthesis method based on a crystal conversion process, which parts from a bulk structure with a different, related crystal structure [4,5]. Here, we will present the detailed electron microscopy analysis of nanotubes and scrolls based on layered CoO_2 that have been obtained using this method with two different starting compounds: $Sr_6Co_5O_{15}$ [4] and $Ca_3Co_2O_6$ [5].

Methods
The synthesis procedure starts from the mentioned bulk oxide materials with a quasi 1D crystal structure, which are treated in a hydrothermal process in basic environment. Under this environment, the structure becomes unstable, leading to the dissolution of Sr (Ca) ions and leaving behind cobalt oxide chains. These chains then bend to 1D tubular or scrolled nanostructures. To investigate these 1D systems, different TEM techniques (HR(S)TEM imaging, SAED, X-EDS and EELS) were performed using two aberration corrected Thermo Fisher Scientific Titan microscopes. Furthermore, the electronic/electrical properties of these nanostructures were investigated in-depth at the individual nano-object level by patterning with electron beam lithography.

Results
A large quantity of strontium deficient misfit $SrCoO_2$-CoO_2 (SCO) nanotubes is produced [4]. In these NTs, CoO_2 layers are stabilized by intercalation between $SrCoO_2$ layers (forming a misfit unit), possibly with the aid of Na ions. In comparison to a previous study on similar nanostructures [3], the NTs obtained by the crystal conversion process are Sr-deficient, yielding a structure predominantly made of CoO_2 layers, Figure (a)-(c). These NTs are semiconducting and possess an extremely high ampacity (10^9 A/cm^2), which is the highest reported ampacity value to date in any inorganic oxide-based material, Figure (d) [4]. The nanotubes also show a breakdown power per unit channel length of 38.3 W/cm, the highest among the regularly used interconnect materials [4].
Regarding the calcium cobaltite (CCO) system, a large quantity of stable and pure CoO_2 nano-scrolls have been produced for the first time and investigated in depth, see Figure (g)-(j) [5]. These NSs possess a narrow range of diameter and wall width suggesting that the CoO_2 stabilization occurs under specific circumstances. These nanostructures are semiconducting with a high current-carrying capacity of 4 10^5 A/cm^2 and an extremely high breakdown voltage of up to 270 kV/cm.

Conclusion

These detailed structural and chemical investigations at the atomic level have demonstrated the existence of new 1D systems based on layered cobalt oxide, both as pure phase and in intercalated form in misfit layered compounds. Furthermore, we have shown that these 1D nanostructures are potential building blocks for high-power electronic applications, fulfilling the requirement suggested by ITRS.

Graphic

Figure: (a) Crystal structures of the Sr-deficient SCO-NTs with intercalated CoO_2 layers: (left) along the cross-sectional direction, and (right) along the a-axis. (b) HRTEM image of a CCO NT. Line profiles show two d-spacings at the NT border, which are attributed to intercalated CoO_2 (0.54 nm) and the SCO misfit structure (0.89 nm). (c) SAED pattern of the NT (inset (b)). Assignment of the different patterns corresponding to the $SrCoO_2$ and CoO_2 subsystems, respectively. (d) Comparison of the ampacity of SCO-NTs (with/without contact resistance) with other inorganic-based semiconductor nanowires/nanotubes (NWs/NTs). (e) Schematic representation of these 1D Nanostructures based on Oxide Misfit Layered Compounds illustrating their outstanding electrical and electronic characteristics. (f) Crystal structure of (left) $Ca_3Co_2O_6$ revealing the separation of Ca and Co columns and (right) schematic representation of a CoO_2 NT and a CoO_2 NS. (g) TEM image showing CoO_2 NS. (h) HRSTEM image of CoO_2 nano-scroll with lattice distances marked. (i) SAED pattern of the CoO_2 NS. (j) Id–Vd curve up to breakdown for the two-probe device (of a CCO NS/NT) shown in the inset.

Funding:
Research supported by the Spanish MICIU (PID2019-104739GB-100/AEI/10.13039/501100011033) and the Government of Aragon (DGA) through the project E13_23R.

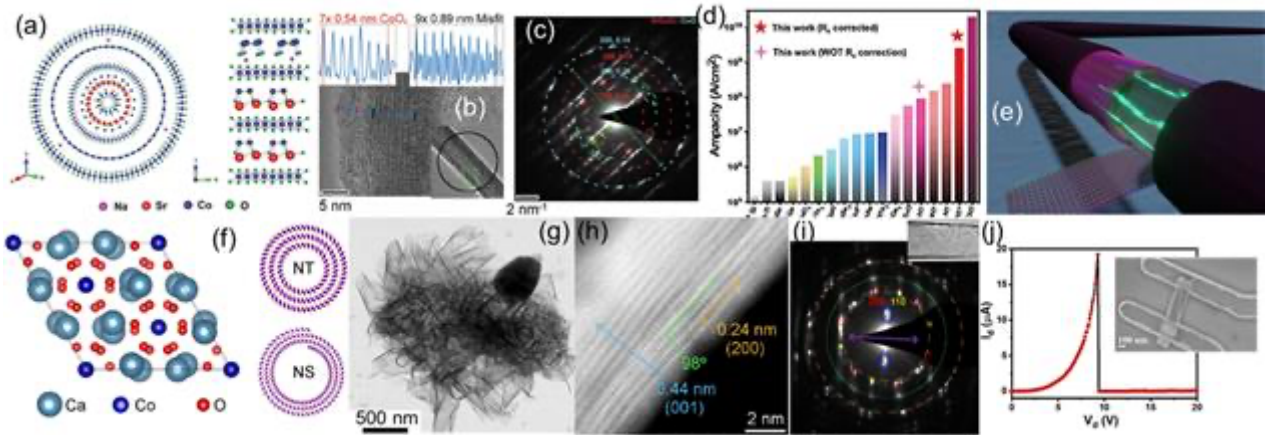

Keywords:

Ceramics, Oxide-misfit-layered-compounds, Nanotubes/Nano-scrolls, Electrical properties

Reference:

[1] M. Serra, R. Arenal, R. Tenne, Nanoscale 11, 8073 (2019).
[2] L.S. Panchakarla, L. Lajaunie, A. Ramasubramaniam, R. Arenal, R. Tenne, ACS Nano 10, 6248−6256 (2016).
[3] L.S. Panchakarla, L. Lajaunie, A. Ramasubramaniam, R. Arenal, R. Tenne, Chemistry of Materials 28, 9150–9157 (2017).
[4] K.S. Roy, S. Hettler, R. Arenal, L.S. Panchakarla, Materials Horizons 9, 2115-2127 (2022).
[5] S. Hettler, K.S. Roy, R. Arenal, L.S. Panchakarla, Submitted.

856

The mixed ionic-electronic conductors studied by advanced transmission electron microscopy

Dr Ke Ran[1,2,3], Dr Fanlin Zeng[4], Dr Liudmila Fischer[4], Dr Stefan Baumann[4], Prof Wilhelm Meulenberg[4,5], Dr Kerstin Neuhaus[6], Prof Joachim Mayer[1,2]
[1]RWTH Aachen University, GFE, Aachen, Germany, [2]Forschungszentrum Jülich GmbH, ER-C, Jülich, Germany, [3]Advanced Microelectronic Center Aachen, AMO GmbH, Aachen, Germany, [4]Forschungszentrum Jülich GmbH, IEK-1, Jülich, Germany, [5]University of Twente, Enschede, The Netherlands, [6]Forschungszentrum Jülich, IEK-12, Jülich, Germany

Poster Group 1

A successful oxygen transport membrane (OTM) requires not only an outstanding permeation performance, but also chemical, electrical, thermal and mechanical stabilities under practical conditions. Among promising candidates, dual-phase OTMs (DP-OTMs) are attracting continuous attention, in which two ceramic phases are coupled to provide mixed ionic-electronic conductivity. In particularly, a fluorite-spinel composite CexGd1-xO2-δ-FeyCo3-yO4 (CGO-FCO) was reported to possess both a significant oxygen permeability as well as a high tolerance under exhaust gas conditions.[1] Thus, considerable efforts have been made to further push the overall performance of CGO-FCO. However, the bottleneck still lies in the inevitable phase interation and the complex grain boundary (GB) structures. In turn, modulating the phase interaction and GB properties offers the possibility of materials engineering, which requires however a precise understanding of the emerging phase and the GBs behaviors down to atomic scale.
In our work, dense pellets of CGO-FCO with different nominal compositions were prepared by solid state reactive sintering.[2] As a result of the phase interaction, an emerging phase with the structure of GdFeO3 (GFO) was often located between CGO phases. Further energy-dispersive X-ray spectroscopy (EDXS) and electron energy loss spectroscopy (EELS) studies revealed varying compositions of the GFO phase, and its formation reduces the Fe and Co segregation at the CGO GBs significantly.[3] Besides, both crystal and chemical structure at the CGO GBs were quantified down to the sub-nm scale, as they are directly related to the ionic conductivity of the membranes.[4] CGO GBs with different coherences were compared. For the Σ3[101] GB in Fig. 1 with a high coherence, only a single layer of Gd segregation can be noticed at the edge of each grain, while the non-solute segregations from Fe and Co are restricted between the two grains. Any variation of the Ce valence state is also largely limited. In contrast, for CGO GBs with a lower coherence, all the atomic-site specific lattice distortions, elemental distributions, and valence state variations were found to be much more significant.
In summary, GFO was identified as the emerging phase within CGO-FCO. Its tunable electronic properties further broaden the opportunity for membrane optimization through phase engineering. Besides, Simultaneous Gd enrichment and Ce depletion within the ending atomic layers of the adjacent CGO grains are generally observed, while Fe and Co are segregated into the CGO GBs with varying amounts and phases. The comparison between GBs with different coherencies indicates that the valence states of Ce, and the enriched Gd, Fe and Co are all sensitive to the local structural defects at the GB. A more coherent GB would thus be beneficial for an improved GB conductivity. Our findings constitute a crucial piece for the complete picture of structure-property relationship of CGO-FCO, which may also shed light on the understanding towards other oxide heterointerface phenomena.

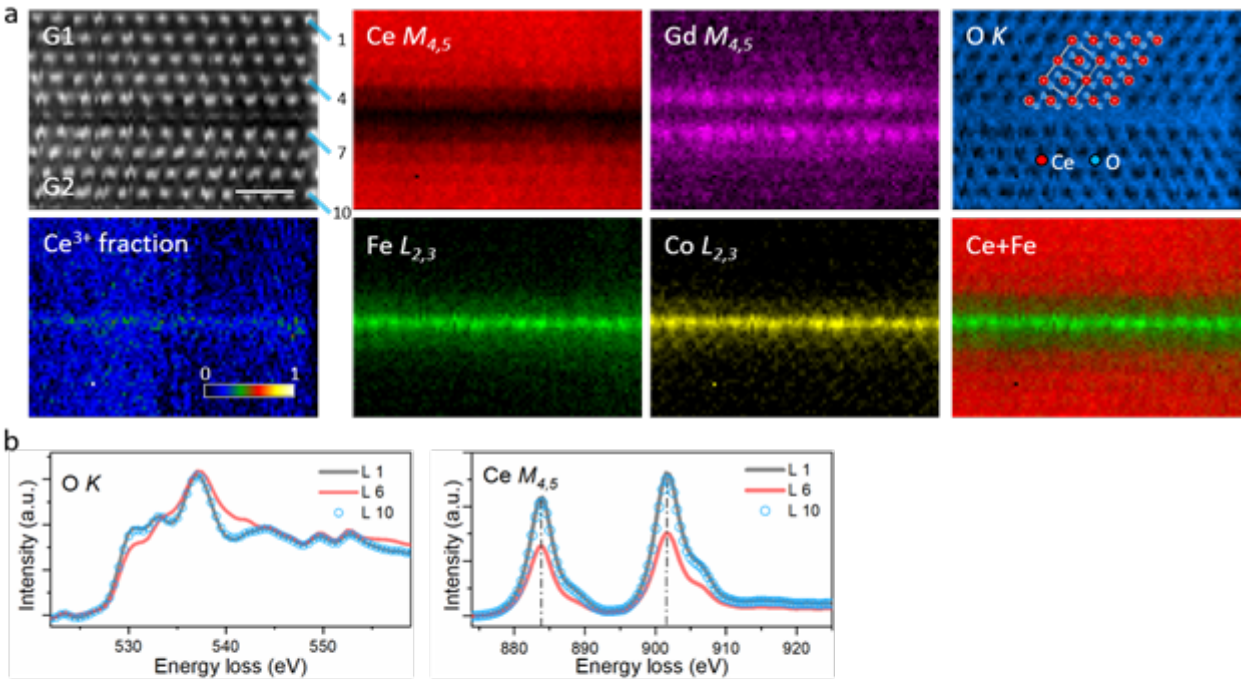

Figure 1. The Σ3[101] CGO GB. (a) EELS SI results: simultaneously acquired ADF image and elemental maps plotting the intensity from the Ce $M_{4,5}$, Gd $M_{4,5}$, O K, Fe $L_{2,3}$, and Co $L_{2,3}$ edges, together with a composite map of Ce and Fe and a Ce^{3+} fraction map. (b) Fine structures of the O K and Ce $M_{4,5}$ edge corresponding to Layer 1, 6 and 10, as labeled in (a).

Keywords:

ceramic membranes, GB-segregation, aberration-corrected TEM

Reference:

1. Y. Lin, S. Fang, D. Su, K. Brinkman, F. Chen, Nat. Commun. 6 (2015) 6824.
2. F. Zeng, J. Malzbender, S. Baumann, A. Nijmeijer, L. Winnubst, O. Guillon, R. Schwaiger, W. A. Meulenberg, J. Eur. Ceram. Soc. 41 (2021) 6539.
3. K. Ran, F. Zeng, L. Fischer, S. Baumann, W. A. Meulenberg, K. Neuhaus, J. Mayer, Acta Mater. 234 (2022) 118034.
4. K. Ran, L. Fischer, S. Baumann, W. A. Meulenberg, K. Neuhaus, J. Mayer, Acta Mater. 226 (2022) 117603.

857

The reversible phase transition of Gd-doped ceria by in situ TEM

Dr Ke Ran[1,2,3], Dr Fanlin Zeng[4], Dr Lei Jin[2], Dr Stefan Baumann[4], Prof Wilhelm Meulenberg[4,5], Prof Joachim Mayer[1,2]
[1]RWTH Aachen University, GFE, Aachen, Germany, [2]Forschungszentrum Jülich GmbH, ER-C, Jülich, Germany, [3]Advanced Microelectronic Center Aachen, AMO GmbH, Aachen, Germany, [4]Forschungszentrum Jülich GmbH, IEK-1, Jülich, Germany, [5]University of Twente, Enschede, The Netherlands

Poster Group 1

Owing to the flexile valence switching between Ce4+ and Ce3+ cations and the facile formation of oxygen vacancies, ceria has been recognized as one of the best candidates for catalysts and solid electrolytes. The formation and migration of oxygen vacancy under external stimuli thus constitute the fundamental processes of the functional oxide materials and their associated devices, which are often linked with modification in the ceria structure and subsequent phase transitions. Typically, ceria crystallizes in a fluorite-type (F-type) cubic structure (space group Fm-3m, a≈5.42 Å). Transition from F-type to the so-called C-type (space group Ia-3) takes place when enough oxygen vacancies are introduced to the system, in Fig. 1. As a result, the cell parameter is doubled, the M site is six-coordinated to O, and the crystallographic positions are split. However, given the challenges in visualizing oxygen dynamics with adequate temporal and spatial resolution, the structural evolution of ceria in response to external stimuli remains rarely explored.[1] Questions pertaining to transition details, including the selection of external stimuli, the behaviors of oxygen vacancies, the feasibility of fine tuning as well as the underlying mechanism remain unsolved.[2]
For our study, the Gd-doped ceria (CGO) with high oxygen ion conductivity as well as giant electrostriction under external electric field is chosen. Dense pellets of Gd-doped ceria were prepared by solid state reactive sintering.[3] The phase transition of CGO is in situ probed down to sub-Å scale by transmission electron microscopy (TEM), where the electron beam (e-beam) is also serving conveniently as an external stimulus. Negative spherical aberration imaging (NCSI)[4] and integrated differential phase contrast (iDPC) imaging are employed, enabling high contrast for both light oxygen and heavy metal atoms, as well as facilitating the measurement of atomic positions with ultra-high precision. Fully manageable transitions are achieved through adjustments to the electron dose rate (EDR). Quantifying lattice distortions also allows a direct estimation of the local oxygen vacancy concentration. The electron energy loss spectroscopy (EELS) reveals varying Ce valence within the CGO. Finally, a collective rearrangement of the oxygen vacancies is proposed to account for our observations, and the simulated HRTEM images show a good agreement with the experimental results. Further numeric calculation would then be necessary to establish a solid theory.
In summary, the reversible phase transitions of CGO were explored in situ with picometer precision. Unique insights into the transition process are gained, such as anisotropic ordering of the oxygen vacancies, direct interpretation of the local oxygen vacancy concentration, and feasible modulation of the transition efficiency. These findings showcase great promise for diverse energy-related applications, including enhancing the performance of ceria-based catalysts and advancing next-generation memristors. The same principle could also be extended to other functional oxides.

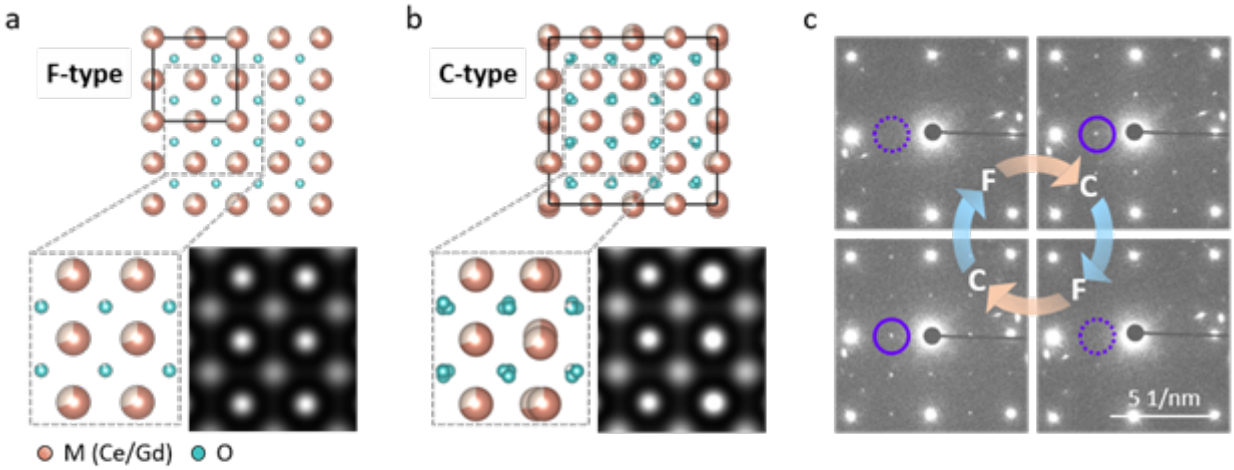

Fig. 1 (a-b) Structural models of the F- and C-type and the simulated HRTEM images. (c) Electron diffraction patterns recorded during a transition cycle. The outlined diffraction spots are only associated with the C-type.

Keywords:

Phase transition, in-situ TEM, NCSI

Reference:

1. L. Zhu, X. Jin, Y. Zhang, S. Du, L. Liu, T. Rajh, Z. Xu, W. Wang, X. Bai, J. Wen, L. Wang, Phys. Rev. Lett. 124 (2020) 056002.
2. X. Li, Z. Liu, A. Gao, Q. Zhang, H. Zhong, F. Meng, T. Lin, S. Wang, D. Su, K. Jin, C. Ge, L. Gu, Nat. Mater. 2024 doi.org/10.1038/s41563-024-01853-9.
3. F. Zeng, J. Malzbender, S. Baumann, A. Nijmeijer, L. Winnubst, O. Guillon, R. Schwaiger, W. A. Meulenberg, J. Eur. Ceram. Soc. 41 (2021) 6539.
4. C. Jia, K. Urban, M. Alexe, D. Hesse, I. Vrejoiu, Science 331 (2011) 1420.

889

Correlation between manufacturing parameters, properties and microstructure in 2D-C/SiC composites

chiara gigante[1], Professor Stefano Poli, PhD Massimiliano Valle, Professor Simone Tumiati, phD Fabio Giacometti, Lorenzo Cavalli, Michela Arnoldi, phD Matteo Boiocchi, phD Yasir Akram, phD Michela Cantù
[1]Earth Science Department A. Desio, Milan, Italy

Poster Group 1

Background incl. aims
C/SiC composites are non-oxide Ceramic Matrix Composites (CMCs) highly sought-after for high-temperature applications in the aerospace industry. These composites consist of a silicon carbide matrix and carbon fibers, which contribute to their excellent mechanical performances.
Although there is common awareness of the influence of raw materials selection - as well as of manufacturing and processing methods - on the thermo-mechanical properties of C/SiC composites, the impact of manufacturing parameters on microstructures is not widely documented in the literature. This is particularly true for C/SiCs produced by means of Liquid Silicon Infiltration (LSI).
Additionally, for many aerospace applications, exposure to oxidative environments is often involved, which can cause material recession due to the rapid oxidation of carbon. Such oxidation can determine a change in the microstructure and a consequent degradation of the mechanical properties. An in-depth knowledge of the microstructure of such composites can help foresee their evolution in oxidative environments and therefore their potential failure in use.
This study focuses on IsiComp® and OxyComp®, two C/SiC composites produced through LSI. Due to the selection of processing parameters, the two composites show different microstructures. IsiComp® has a laminate structure, in which fiber bundles are wrapped by the SiC matrix. In OxyComp® the SiC matrix penetrates within the fiber bundles and the ceramic matrix is highly cross-linked, almost resembling the microstructure of a pure ceramic. Despite its peculiar microstructure, OxyComp® has good mechanical properties and shows a pseudo-ductile behavior under stress, which is unusual, considering that ceramics retain a brittle behavior under mechanical stress.
In this frame, this research aims to quantify microstructural changes due to varied manufacturing parameters and their impact on microstructures, and therefore, on the thermo-mechanical properties of the composites. Another aim is to delineate the property and microstructure evolution during oxidation in aerospace-like environments - including vapor-rich combustion-type atmospheres. Understanding these relationships is crucial to predicting the behavior of C/SiCs under operating conditions and selecting the most suitable material for certain applications.

Methods
Samples are produced using vacuum bagging techniques, then pyrolyzed and converted into a CMC via LSI. Physical, thermal, and mechanical properties (bending) were tested before and after exposure to oxidative environments according to standard procedures.
Oxidation experiments were conducted in a vertical furnace equipped with a water vapor-gas mixing system and a Quadrupole Mass Spectrometer (QMS) for the in-situ analysis. The structural evolution is quantitatively described using 2D electron microscopy images and 3D images from X-ray tomography. Image analysis is conducted using quasi-automated tools provided by Fiji and Wolfram Mathematica.

Results
As for IsiComp®, the molding pressure strongly affects the size of residual pores in the pyrolyzed preform and the thickness of the ceramic channels in the CMC. The higher the molding pressure, the

higher is number of thin (typically less than 30 µm) vertical fractures in the pyrolyzed preform, and no large pores are observed. This enhances silicon infiltration, leading to a homogeneous LSI microstructure. Circular isolated pores resulting from gas generated during the resin polymerization can be eliminated by adjusting the curing cycle parameters.
Surprisingly enough, despite processing parameters having a strong impact on the texture of the pyrolyzed preform, no major effect can be detected in terms of thermal and mechanical properties of the CMC after LSI.
Under oxidative conditions, ISiComp® performs similarly to 2D-C/SiCs described in the literature.
As for OxyComp®, the fiber-to-matrix ratio within pyrolyzed preforms can be tuned by changing certain processing parameters, which eventually affect the pervasiveness of silicon penetration during LSI. The size distribution of SiSiC channels in the CMC reflects the intensity of silicon penetration within fiber bundles. The higher the fraction of thin channels (<7.5 µm-thick), the greater the residual deformation under a fixed mechanical stress. Thermal properties are less affected by the extent of silicon penetration within fiber bundles, as they are more influenced by the continuity of ceramic matrix in a specific direction.
Thanks to its microstructure OxyComp® performs very well under oxidative conditions.
For both composites, it was observed that prolonged exposure at relatively low temperatures causes intra-bundle fiber oxidation, which undermines both material integrity and mechanical properties more strongly than short-term exposure at higher temperatures does.

Conclusion

This study investigates the relationship among manufacturing/processing parameters, microstructures, and thermo-mechanical properties of IsiComp and OxyComp, two C/SiC composites developed by Petroceramics S.p.A.
The manufacturing pressure significantly influences the microstructure of ISiComp®, but no major effects were observed in terms of mechanical and thermal properties measured. It can be supposed that the observed differences in the pyrolyzed preform are attenuated in the CMC, which indicates the final material is highly reproducible despite any difference in the processing parameters.
Conversely, variations of the microstructure of OxyComp® strongly affect its mechanical behavior (bending) but have a weaker impact on the thermal conductivity. The effect of differences in the texture of OxyCOmp® on the oxidation resistance is still under investigation.
The microstructural description derived from 2D-SEM images is consistent with the one obtained from 3D X-ray tomography images.
The pervasive presence of SiC matrix within the fiber bundle makes OxyComp® better oxidation-resistant than ISiComp®, both in air and in a H2O-vapor-saturated atmosphere.
OxyComp shows superior oxidation resistance compared to IsiComp, mostly due to thin intra-bundle channels which slow down the oxidation progression. For both composites, it was observed that prolonged oxidation at relatively low temperatures has a major impact on the mechanical properties of the composite in use.

2D - IsiComp®

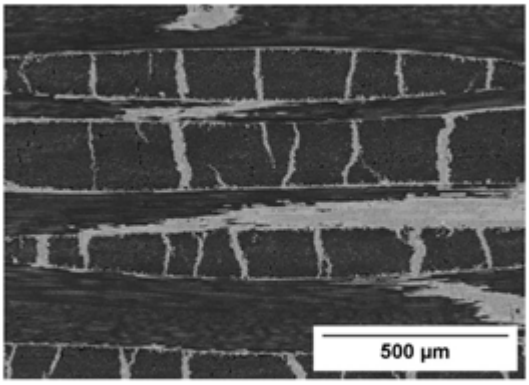

2D - Oycomp®

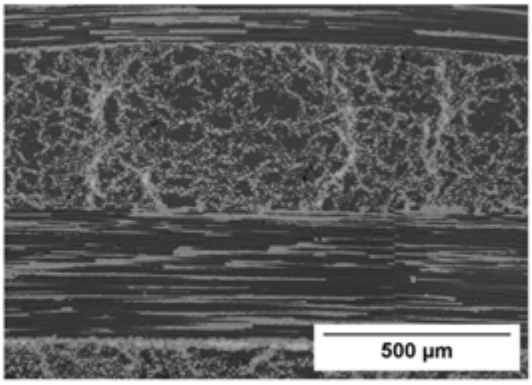

Keywords:

CMCs, microstructural description, thermo-mechanical properties

Reference:

Lehnert, T., Heidenreich, B. & Koch, D. Investigation of process influences on the amount of single-fiber siliconization in C/C–SiC samples by machine-learning methods. Open Ceram. 15, 100383 (2023).

Galizia, P. & Sciti, D. Disclosing residual thermal stresses in UHT fibre-reinforced ceramic composites and their effect on mechanical behaviour and damage evolution. Compos. Part B Eng. 248, 110369 (2023).

Niu, Z. B. et al. A damage constitutive model for the nonlinear mechanical behavior of C/SiC composites during mechanical cyclical loading/unloading. Compos. Part A Appl. Sci. Manuf. 161, (2022).

Reimer, T., Petkov, I., Koch, D., Fließ, M. & Dellin, C. Fabrication and characterization of C/C-SIC material made with pitch-based carbon fibers. Ceram. Trans. 252, 277–293 (2015).

929

The effects of TiC network microstructure on the mechanical properties of spark plasma sintered Al2O3

Umut Savaci[1], Salih Cagri Ozer[1], Eren Can[1], Yiğit Berkcan Harmankaya[1], Servet Turan[1,2]
[1]Eskisehir Technical University, Department of Materials Science and Engineering, Eskisehir, Turkey,
[2]Ceramic Research Center, Eskisehir, Turkey

Poster Group 1

Background incl. aims
Al_2O_3-based composite materials are widely used for cutting tool applications due to their high strength, hardness and wear resistance. Despite these ideal mechanical properties, having low fracture toughness values and brittleness present problems during application. This study aimed to improve both the hardness and fracture toughness of Al_2O_3 simultaneously by taking advantage of different mechanisms with TiC network structures. Hardness was aimed to be increased by introducing the TiC secondary phase with high hardness throughout the Al_2O_3 matrix. On the other hand, fracture toughness was aimed to be improved by promoting crack deflection mechanisms by the formed network structure.
Methods
Al_2O_3 ceramics with TiC network microstructures were produced by the spark plasma sintering (SPS) technique by coating the Al_2O_3granules with 2-10 vol.% TiC powders, utilizing a simple dry coating method. The sintering process was carried out at a minimum of 1400°C dependent on the TiC content. The effects of various amounts of TiC addition and differing sintering temperatures on the microstructural and mechanical properties of Al_2O_3 were observed by scanning electron microscopy techniques as well as mechanical testing.
Results
Network structures of TiC were formed successfully around the Al2O3 matrix during the SPS process, resulting in simultaneous improvement of hardness and fracture toughness. Present TiC and Al2O3 phases were confirmed by the X-ray diffraction analysis. The fracture toughness of Al2O3 was improved by crack deflection and bridging mechanisms induced by the introduction of the network structure, as observed by the microstructural investigations. In addition, Vickers microhardness values of the samples were found to be increased with increasing volume fraction of TiC.
Conclusion
As a conclusion, in this study, mechanical properties of the Al2O3 ceramics were successfully improved by the formation of TiC network around Al2O3 granules. Electron microscopy studies revealed the formation of the continuous network around the matrix and microstructural features such as grain size, and porosity as well as toughening mechanisms.
This study was supported by Eskişehir Technical University Scientific Research Projects Commission under grant no 23ADP195

Keywords:

Al_2O_3, TiC, Network, SPS, Properties

1006

FIB-SEM/microtoming prepared Cross Section of a Stone Wool Fiber enabling (S)TEM investigation

Phd Student Krestine Hofstedt Rasmussen[1,2], Ph.D Denis V. Okhrimenko[2], Ph.D Louise J. Belmonte[2], Ph.D Dorthe B. Ravnsbæk[3], Ph.D Espen D. Bøjesen[1]
[1]Interdisciplinary Nanoscience Center, Aarhus University, Aarhus, Denmark, [2]ROCKWOOL A/S, Hedehusene, Denmark, [3]Department of Chemistry, Aarhus University, Aarhus, Denmark

Poster Group 1

Stone Wool Fibers (SWFs) are aluminosilicate fibers widely used for building and housing insulation. Rocks are melted in a high-temperature furnace (~1500°C) and spun into elongated and cylindrical amorphous fibers approximately 5 µm in diameter and 2 mm in length [1]. ROCKWOOL is a world leading producer of mineral wool fibers used for building and housing insulation. ROCKWOOL continuously transitions to a greener production. This transition potentially influences the redox chemistry and thus the atomic scale network, which consequently could influence the fire resilient properties of SWFs. Our goal is to create a thin (approx. 40-140 nm) cross section of a single stone wool fiber to be able to obtain sub-nanometer scale structural and compositional information using (scanning) transmission electron microscopy ((S)TEM) based techniques. Only by exploring and understanding the structure of SWFs on all length scales (micro, nano, and atomic), will we fully be able to understand the mechanisms behind the fire protective properties of SWFs.
Current strategies used by ROCKWOOL to prepare cross sectional samples include mechanical polishing of SWFs embedded in an epoxy matrix. However, this technique is not suitable for STEM-based investigations due to the large sample thickness and the high likelihood of surface contamination caused by polishing. Thus, a new approach for thin sectioning optimal for (S)TEM analysis is needed. A major obstacle to obtaining the sought-after cross-section cross section is the non-conductive nature of the SWFs. Here, we present the current state of our exploration using focused ion beam scanning electron microscopy (FIB-SEM) and testing of using ultra-microtoming of fibers cast into an epoxy matrix for the preparation of cross sections of SWFs for further (S)TEM investigations. While bombarding the fiber with ions in the milling process, high precision is obtained by continuously monitoring and guiding the process by scanning the electron beam across the area of interest [2,3]. The non-conductive nature of the fibers will lead to build up of charge on the fiber surface and may cause deflection of the beam that otherwise enables the high-resolution imaging, which ensures a precise milling process. The cross-sectional lamella is prepared using a FEI VERSA 3D FIB-SEM system equipped with a Gallium ion source or a Leica EM UC7 ultra-microtome with a diamond knife. In our approach, the fibers for FIB-SEM are carefully placed in/on carbon paste that is added to a silicon wafer. Hereafter, the fibers are coated with 600 nm gold (Au) to shield the fiber throughout the milling process. Preliminary results have shown that optimal conditions for the milling include a low I-beam current of a maximum of 5 nA to avoid damage to the fiber upon sputtering.
Furthermore, the tilt angle used to properly clean and mill the thin section of a fiber is further under improvement. Currently, tilt angles of 50.5° and 53.5° are used as the FIB column is located at 52°. In general, the aim is to estimate the right trade-off between acquiring optimal imaging and milling without too much charge build up on the specimen [4]. A test of using ultra-microtoming for thin sectioning is investigated simultaneously to acquire the best possible cross section. This technique also ensures that no damage to the structure of the fiber is created as with FIB-SEM might lead to. A thin section of approx. ~40 nm was acquired with microtoming and initially investigated in STEM mode using a TESCAN Clara scanning electron microscope. Both techniques show promising initial results on our way to creating a thin cross section of fiber. However, both techniques also show some obstacles to overcome in the process. For FIB, damage upon sputtering should preferably be avoided

and strategies to minimize charging need to be optimized. For microtoming, a major current obstacle is to optimize the mechanical properties of the epoxy to match those of the fibres to optimize the cutting process. The process of acquiring this cross section for TEM investigations is still in the primary stages, focusing on practicing the lift-out process of the cross section and mapping out the charging effects.

Keywords:

Stone Wool, aluminosilicates, FIB-SEM, TEM

Reference:

[1] J. E. Shelby, Roy. Soc. Chem., 2021, 3rd ed.;
[2] R. M. Langford, Microsc. Res. Tech., 2006, 69(7), 538-549; [3] L. A. Giannuzzi and F. A. Stevie, Micron, 1999, 30(3), 197-204;
[4] D. C. Joy and C. S. Joy, Micron, 1996, 27(3-4), 247-263

1015

The Development of Japanese ceramic ware (pottery and porcelain) Technology as Revealed by EPMA

Dr Rie WAKIMOTO[1], Dr Susumu KAKUBUCHI[2], Dr Sergei Matveev[3]
[1]JEOL Ltd., Musashino Akishima, Japan, [2]SAGA University, SAGA , Japan, [3]JEOL (GERMANY) GmbH, Gute Aenger, Germany

Poster Group 1

Introduction

The quality of Japanese ceramics ware has improved dramatically since the importation of advanced ceramics, especially percaline technology from the continent in the 17th century. In particular, Old Imari, (Ko-Imari), made after the 17th century using highly refined continental techniques, was loved by celebrities not only in Japan but around the world [1]. Of course, even before the 17th century, ancient Japanese pottery techniques had developed and many potteries were produced.
This report describes an observation and analysis of the development of medieval ceramics in Japan before and after the high level of ceramic ware technology was introduced.

Methods

The samples for analysis were pieces collected from the Chita kiln site [2] of Paleo-Tokoname, old pottery ware (early Sengoku period (late 800s)), the Komizo kiln site of early Arita porcelain ware (early 1600s), and the Kakiemon kiln site (late 1600s) [3] where ceramic porcelain technology was established. Thin sections were created by gluing a small piece of pottery onto a glass slide, and then grinding it. The thin sections were observed and analysed with an electron probe microanalyser (JEOL JXA-iHP200F).

Results

The backscattered electron (compositional) image (BEI) and the panchromatic cathodoluminescence (CL) image and Si mapping analysis results are shown in Figure 1. The upper part of the BEI shows the glazed part of the ceramic surface. The glazed width of the paleo Tokoname piece (Very initial period) (a) is thin and contains many impurities. Also, the Komizo piece (early period) (b) contains many impurities in the glaze, whereas the Kakiemon piece (established period) (c) contains fewer impurities. The panchromatic cathodoluminescence (CL) images show strong luminescence in the glazed areas of the Tokoname piece and the Komizo piece. On the contrary, no CL luminescence is observed in the Kakiemon piece glaze part. Also, the base of Tokoname piece shows stronger CL luminescence than the Komizo and Kakiemon pieces. Si mapping results show that the impurities in the glaze of the Tokoname piece and Komizo piece include Si-particles (Single arrows in the figure), indicating that many quartz fragments are still present. On the other hand, in the Kakiemon piece, these mineral particles are not found.

.

Conclusion

The BEI and CL images and Si maps show that the glaze width of the Tokoname piece is thin and contains many impurities, indicating that the glaze firing technique is immature. Normally, pottery are made from low-glassy materials, while porcelain is made from high-glassy materials. Strong CL luminescence in the base of Tokoname piece indicates a high content of crystalline quartz fragments. The glaze width of the Komizo piece is well present, on the other hand Si and CL strong luminescence is observed in the glaze area, suggesting that early Arita ware glaze still contains unmelted quartz. In the Kakiemon, glaze width is sufficient and these mineral particles are not found. These results suggest that the Kakiemon ware was produced at higher temperatures with better quality glaze than the Tokoname ware and Komizo ware was due to the development of pottery techniques. In other

words, Japanese ceramics technology has improved at a very fast pace in just 100 years since the importation of pottery technology developed from the continent in the early 1600s.

Figure 1. BEI, CL images and Map analysis results. (a) Paleo Tokoname piece. (b) Komizo piece. (c) Kakiemon piece. Si grains with strong CL luminescence are identified in the Tokoname and Kamizo glaze parts (single arrows).

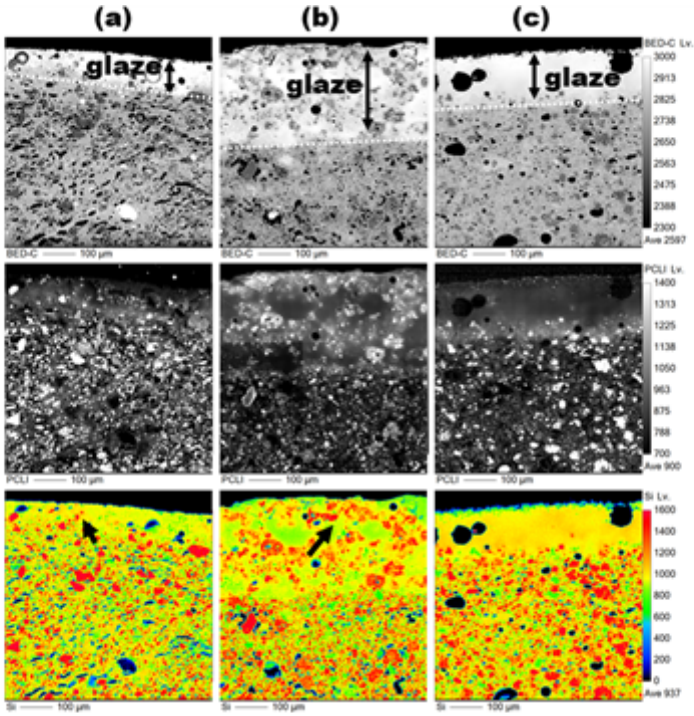

Keywords:

Old Imari, Map Analysis, CL

Reference:

[1] Heibon-Sya 2000 Pottery Encyclopedia. (ISBN 9784582129199)
[2] Tokoname Ceramics Magazine, Tokoname City Magazine, Supplement Volume, 422.
[3] Museum of History and Folklore of Arita 1991 Arita-yaki Research Report Seikaido.

1016

Relative thickness study of TEM samples

Dr Sandra Drev[1], Petra Drnovšek[1], Dr Miran Čeh[1,2]
[1]Center for Electron Microscopy and Microanalysis, Jožef Stefan Institute, Ljubljana, Slovenia,
[2]Department for Nanostructured Materials, Jožef Stefan Institute, Ljubljana, Slovenia

Poster Group 1

Sample preparation methods have an important role in transmission electron microscopy (TEM). New materials (ceramics, thin films, composites, etc.) that are now present have a specific property and have to be precisely treated and usually post-treated. This poses ever-new challenges, constant adjustments, and improvements in advanced TEM preparation techniques like focused ion beam sample preparation, conventional sample preparation, and other TEM preparation methods.
In this paragraph, we compared two nowadays most frequently used TEM sample preparation techniques; conventional sample preparation and focused ion beam sample preparation. TEM samples were, in the last stage of preparation, final-treated using NanoMill® (model 1040, Fischione Instruments, Inc.) to achieve the best results for further TEM/STEM analysis. The study was created for a discussion about using different approaches to achieve the best result for the TEM sample preparation.
The first TEM sample was prepared using FEI Helios NanoLab NL650 dual-beam Focused Ion Beam (FIB). The sample was finally treated (thinned and cleaned) with NanoMill under specific conditions for FIB-type samples. The second TEM sample was conventionally prepared. The sample was thinned, dimpled down to transparent thickness (Dimple grinder, Gatan Inc.), and ion-milled using PIPS (Precision Ion Polishing System, Gatan Inc.) to achieve perforation. In the last stage, the sample was finally treated with NanoMill under specific conditions for conventional-type sample preparation.
We want to expose how important is to choose the proper technique and appropriate conditions for TEM sample preparation. Relative thickness study distinctly revealed improvement in sample quality that affects the final STEM investigations.

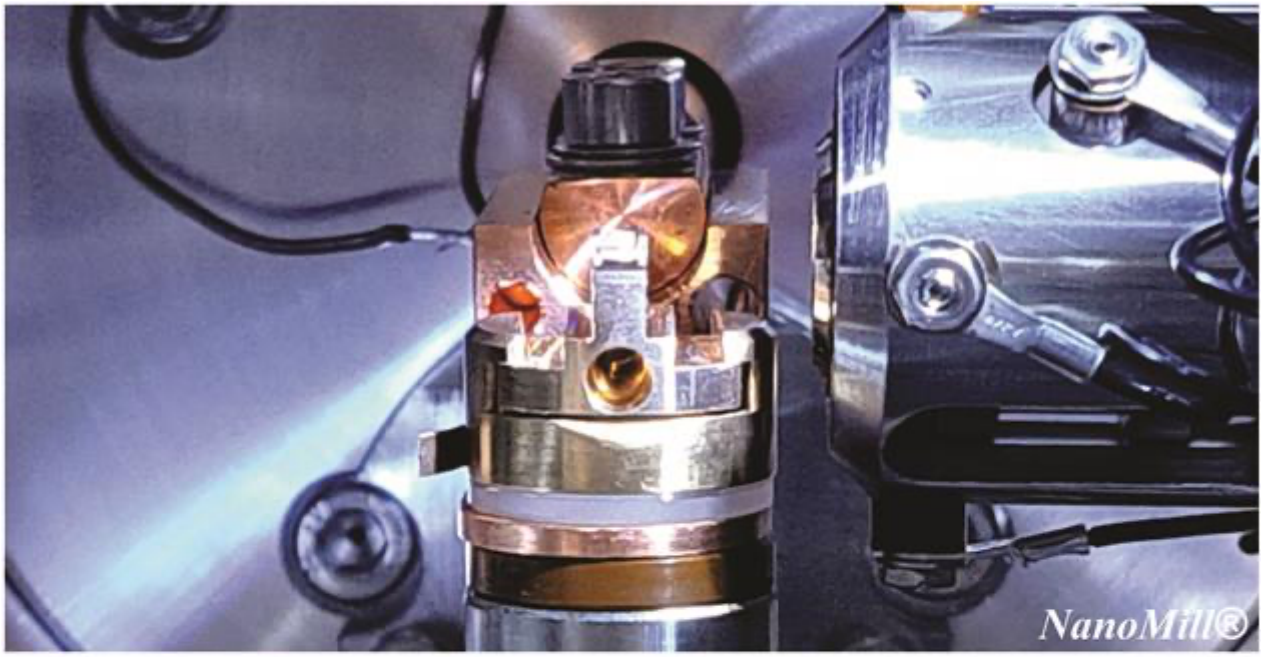

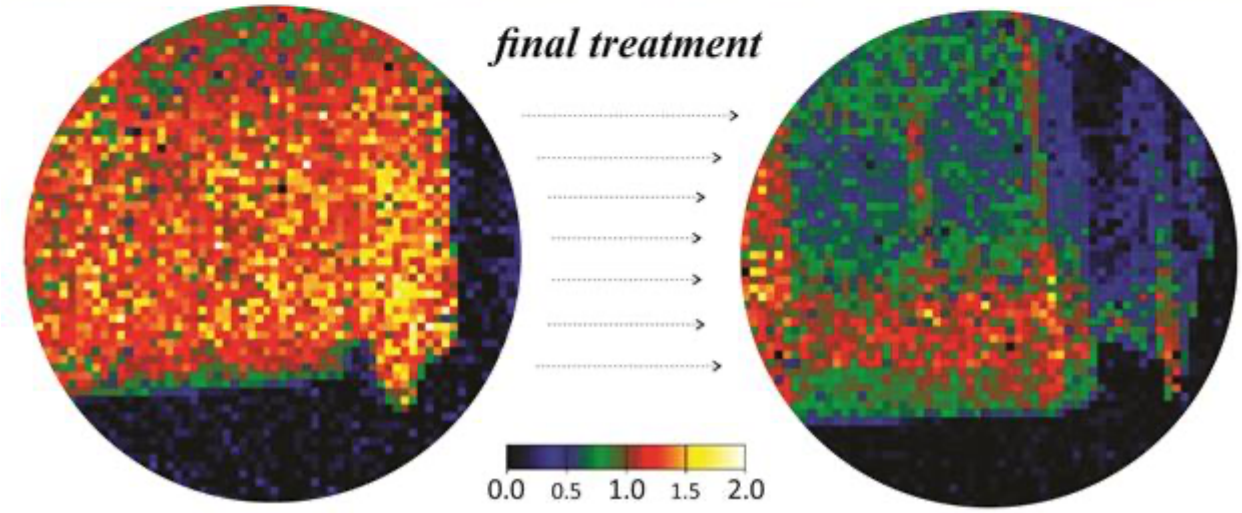

Keywords:

TEM, NanoMill, FIB, conventional TEM

1048

The effects of B4C network microstructure on the thermoelectrical properties of spark plasma sintered SiC

Dr Salih Cagri Ozer[1], Ceren Korler[1], Prof. Dr. Servet Turan[1,2]
[1]Eskisehir Technical University, Department of Materials Science and Engineering, Eskisehir, Turkey,
[2]Ceramic Research Center, Eskisehir, Turkey

Poster Group 1

Thermoelectric (TE) devices convert waste heat to electricity and can be used in industrial waste heat recovery utilizing TE materials which may play a vital role in developing sustainable and renewable energy-harvesting technologies. TE materials should have high electrical conductivity and Seebeck coefficient as well as low thermal conductivity for a high dimensionless figure of merit, ZT, which represents the efficiency of TE conversion. Since these properties are related to each other, e.g. a high electrical conductivity results in a high thermal conductivity value, different composite approaches or doping must be maintained for optimization of these properties. Our recent studies explored the effects of transitional metal carbide/boride network microstructures on the TE properties of SiC and B_4C which revealed simultaneous improvement of electrical and thermal conductivities with conductive network and increased phonon scattering, but deterioration of the Seebeck coefficient due to the metallic nature of the network microstructure. To minimize this problem, a B_4C network microstructure was implemented to the SiC matrix in this study, aimed to increase the electrical conductivity with minimal Seebeck coefficient loss thanks to the semiconductor nature of B_4C.

Polycrystalline bulk samples of SiC with B_4C network structures were prepared by a simple dry particle coating method followed by spark plasma sintering (SPS). 1–8 vol.% B_4C-coated SiC granules were consolidated in an SPS furnace (HP 25D, FCT GmbH, Germany) at 2000°C by applying 40 MPa pressure under a vacuum atmosphere with a 5-minute holding time. Phase and microstructure analyses were carried out on polished surfaces of the sintered bulk samples. Electrical conductivities and Seebeck coefficients of the samples were measured simultaneously by the four-point probe method between 323 and 923 K. Thermal diffusivity and heat capacity values were measured by the laser flash analysis and differential scanning calorimetry, respectively, to calculate the thermal conductivity. Density values were obtained by using the Archimedes method at room temperature.

The implementation of the conductive B_4C network microstructures given in the figure (light phase is SiC matrix, dark phase is B_4C network) improved the electrical conductivity of SiC simultaneously with the decrease in thermal conductivity due to the increased phonon scattering with increased grain boundary concentrations. Optimization of B_4C content resulted in a minimal decrease in the Seebeck coefficient resulting in a composite with increased ZT values and TE performance.

To conclude, SiC granules were successfully coated with 1–9 vol.% B_4C powders and then spark plasma sintered to obtain conductive B_4C network microstructures to improve the TE performance of SiC by simultaneously increasing electrical and decreasing thermal conductivities while limiting the decrease in the Seebeck coefficient to a minimum.

This study was financially supported by the Scientific and Technological Research Council of Turkey (TUBITAK) (219M514) and The Eskisehir Technical University Scientific Research Project (23ADP195).

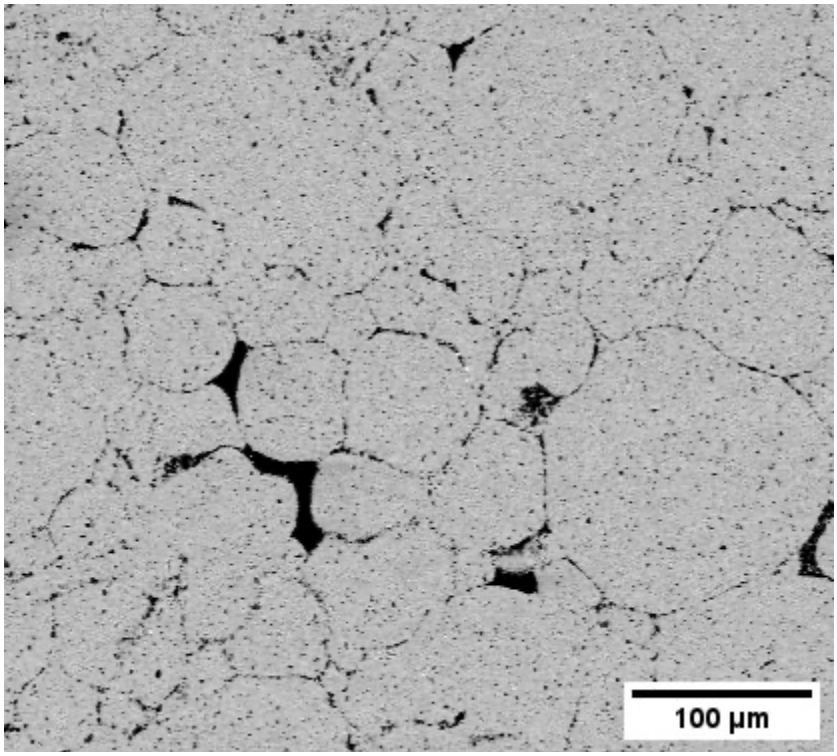

Keywords:

SiC, B_4C, Network-microstructure, SPS, Thermoelectric

Reference:

Ozer, S.C., Arslan, K. & Turan, S. Thermoelectric properties of carbide ceramics:a comparative analysis of thermoelectric properties of B_4C, SiC and TiC. Journal of the Australian Ceramic Society 60, 407–418 (2024). https://doi.org/10.1007/s41779-023-00979-4

Ozer, S.C., Arslan, K. & Turan, S. Improved thermoelectric properties of SiC with TiC segregated network structure, Journal of the European Ceramic Society, 43 (14), 6154-6161 (2023). https://doi.org/10.1016/j.jeurceramsoc.2023.05.050.

Ozer, S.C., Arslan, K. Metin, E. & Turan, S. The effect of in-situ TiB_2 segregated network structure on the thermoelectric properties of spark plasma sintered B_4C ceramics, Journal of the European Ceramic Society, 43 (16), 7508-7515 (2023). https://doi.org/10.1016/j.jeurceramsoc.2023.08.005.

1087

Observing the in-situ formation of the lead-free piezoceramic potassium sodium niobate (KNN) with SAED

Dr Mark Rambaran[1], Dr Daniel Jacobsson[1,2], Dr Sebastian Lehmann[3], Prof. Kimberly Dick[1]
[1]Centre of Analysis and Synthesis and NanoLund, Lund University, Lund, Sweden, [2]National Centre for High Resolution Electron Microscopy , Lund University, Lund, Sweden, [3]Division of Solid State Physics and NanoLund, Lund University, Lund, Sweden

Poster Group 1

Background incl. aims
The use of PZT has continued despite the restriction of hazardous substances (RoHS) directives being passed by the European union (EU) to limit the use of hazardous materials – such as lead (PZT) – in electronic equipment. This is influenced by a lack of available substitutes that can be implemented and scaled in a reasonable time to eliminate the use of PZT (RoHS Annex III). The lead-free alkali-niobate, potassium sodium niobate (KxNa1-xNbO3, KNN), is a potential replacement for PZT, since it can exhibit equivalent, if not better, piezoelectric properties without compromise at temperatures >120 °C. The challenges in the synthesis of KNN, however, have hindered its use as an alternative. Notable challenges include difficulty in achieving the 50% K+ and Na+ occupancy required to make stochiometric KNN (i.e., K0.5Na0.5NbO3) and a lack of control in the formation of phase boundaries. Therefore, developing a reproducible method for synthesising stoichiometric KNN, bodes well for the implementing KNN as a commercial piezoceramic.

Methods
A simple and robust method for synthesis of the lead-free piezoceramic material KNN has been developed via an aqueous route. Stochiometric KNN (K0.5Na0.5NbO3) was prepared by combining alkali-nitrate solutions (NaNO3 and KNO3) with the nano-sized, water-soluble, niobium precursor hexaniobate ([HxNb6O19]8-x, Nb6), followed by sintering at elevated temperatures. Ex-situ studies on the formation of solid-state niobium oxides from Nb6 indicate formation of amorphous niobium oxides ca 400–500 °C. However, observing the dynamics accompanying this crystallization process are limited with conventional solid-state methods. We therefore probed the transformation of Nb6 in the presence of alkali-cations, to yield crystalline KNN from an amorphous oxide precursor. This was possible via in-situ heating with simultaneous selected area electron diffraction (SAED). Whereby, the amorphous Nb6-KNN precursor was mounted on a micro-electromechanical systems (MEMs) chip (Norcada Inc.), which is heated via a tungsten filament coil. In-situ heating experiments proceeded with heating from 400 to 1000 °C, at ramping rate of ca 0.25 °C s-1 in vacuum.

Results
KNN can be synthesised with heating NaNO3 and KNO3, with the water-soluble hexaniobate (Nb6) precursor. The results from SAED indicate the amorphous Nb6-KNN precursor becomes crystalline above ca 550 °C, without degradation after further heating up to 1000 °C. The SAED patterns at 800, 900 and 1000 °C, were acquired along the (101) axis, and agreed with the simulated diffraction pattern of stoichiometric KNN reported previously. The SAED patterns <800 °C exhibited sporadic spots which were incongruent with the simulated diffraction pattern. However, below ca 550 °C there were no obvious spots in SAED patterns, which is consistent with the presence of an amorphous oxide. These findings merit the use of a water-soluble niobium precursor, such as Nb6, as an alternative to accessing KNN in the solid-state.

Conclusion

In-situ heating with SAED is a suitable technique for monitoring the real-time transformation of amorphous precursor oxides, to yield crystalline lead-free piezoceramics. Formation of the lead-free piezoceramic KNN is achievable using the water-soluble, niobium precursor Nb6, which is advantageous compared to conventional solid-state methods. This makes it an attractive alternative approach for developing lead-free piezoceramic materials.

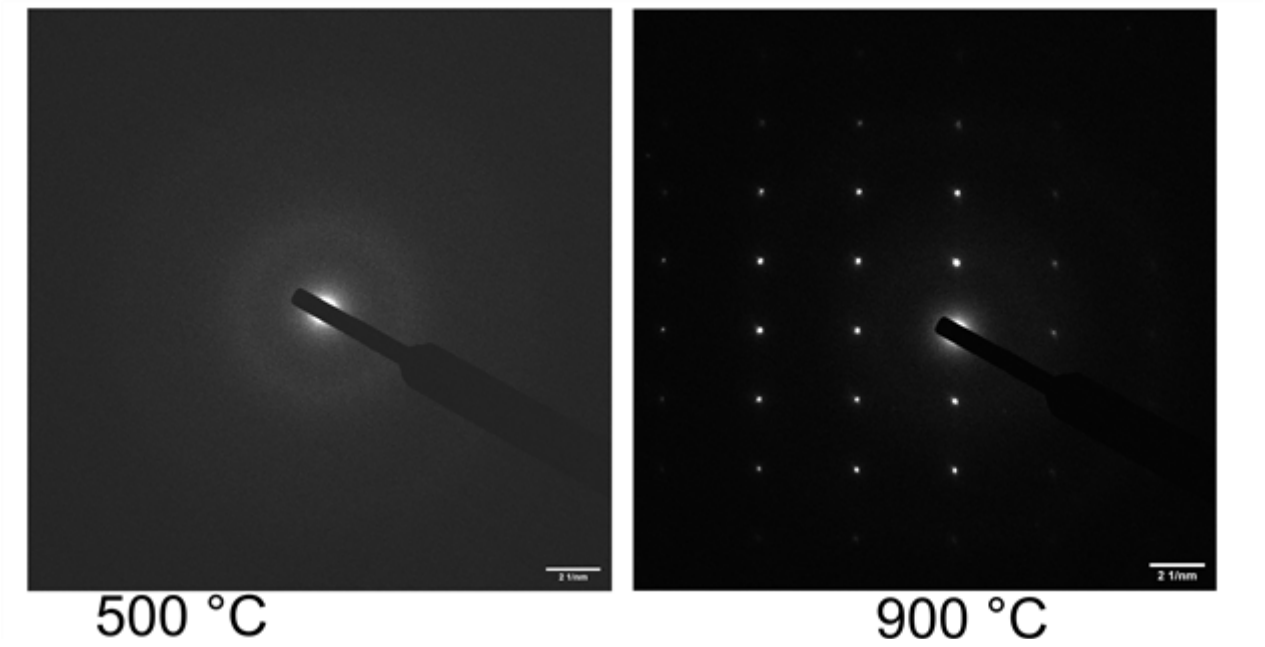

Keywords:

Lead-free, hexaniobate, KNN, in-situ, TEM

Reference:

Reference:
[1] M. A. Rambaran, A. Gorzsás, M. Holmboe, C. A. Ohlin, Dalton Trans. 2021, 50, 16030-16038.
[2] M. A. Rambaran, M. Pascual-Borràs, C. A. Ohlin, Eur. J. Inorg. Chem. 2019, 3913-3918.